# NON-INVASIVE DETECTION OF SOIL MOISTURE IN WET VERTISOLS USING ELECTRICAL RESISTIVITY TOMOGRAPHY

A Thesis

by

ELIZABETH GRACE MARLEY

Submitted to the Office of Graduate and Professional Studies of
Texas A&M University
in partial fulfillment of the requirements for the degree of

MASTER OF SCIENCE

| | |
|---|---|
| Chair of Committee, | John Alexander Thomasson |
| Co-Chair of Committee, | Cristine Lois Smith Morgan |
| Committee Member, | Yufeng Ge |
| Head of Department, | Stephen W. Searcy |

August 2018

Major Subject: Biological and Agricultural Engineering

# ABSTRACT

The unique characteristics of Vertisols complicate soil moisture measurements and often obscure traditional markers of wetland soils, which may result in failure to identify jurisdictional wetlands. Electrical Resistivity Tomography (ERT) has been proposed for non-invasive measurement and temporal monitoring of soil moisture in Vertisols. Resistivity measurements were conducted on two Texas Vertisols: a Typic Hapludert and a Chromic Haplustert. Water and clay content were determined from soil cores taken from corresponding ERT transects. Multiple linear regression models predicting volumetric water content from log resistivity and clay content indicate that resistivity is, at best, a weak predictor of water content in high-clay soils (p-value $\geq$ 0.03), while clay content is consistently highly significant (p-value $<$ 0.001). Further, regression models were site-specific. Regression of changes in log resistivity and water content over time provides weak evidence that ERT may be used to monitor temporal trends. Resistivity was a significant predictor of changes in water content (p-value $<$ 0.001) in a limited area at one site where clay content was well-known and changes in both resistivity and water content were large compared to other areas in the same site. Changes in soil moisture cannot be accurately quantified from changes in resistivity in wet Vertisols, though wetting and drying trends may be discernible. ERT data in wet Vertisols are prone to noise that obscures the signal from soil moisture. Accordingly, ERT is generally unfit for monitoring temporal changes in soil moisture in wet Vertisols.

# ACKNOWLEDGMENTS

I am most grateful to have been part of the BAEN family for over a decade. I recognize that having talented professors, administrators, and staff who genuinely care about their colleagues and students is a privilege. We have been together through personal and collective ups and downs, and the love and support of our departmental family has helped us through it all. Thank you to our Department Head, Dr. Searcy, for encouraging our family atmosphere and for always asking me when I was finally going to graduate. I think I have an answer now.

Thank you to my committee – Dr. Thomasson, Dr. Morgan, and Dr. Ge – for your extraordinary patience, care, and guidance throughout my graduate career. All three of you are true role models both professionally and privately. Without your encouragement as well as your concern for me personally I would not have been able to finish this work. Thank you for going above and beyond in your commitment to your students' academic success and personal wellbeing.

Thank you to the student workers and fellow graduate students who have helped, mentored, and commiserated with me over the years. Chase Vasbinder and Jose Fuentes are some of the hardest and most cheerful workers I have ever met. Haly Neely and Dianna Bagnall are truly dedicated to their work and to their people. Jason Ackerson's experience and advice in my research area were foundational to my success. Mijin Seo

and Jianing He have been constant and dear friends as we muddled through graduate school together.

Thank you to my family and friends for continuing to encourage and put up with me through my seven years of graduate school. When it seemed like I would never finish, you lovingly reminded me that I had to, and did whatever you could to help motivate me to the finish line. Thank you to my husband for keeping me fed, helping me with MATLAB problems, listening to me complain, and insisting that I am capable of this work and deserving of this degree even when I didn't feel like it.

Thank you to my Deaf Church community for praying for me through all the ups and downs of grad school and of life. It is a blessing and a joy to have been part of such a loving group of people. Thank you also to my Grace Bible Church community for many years of wise counsel, solid teaching, and tangible demonstration of what it means to follow Christ.

I thank God for all I have learned, accomplished, and experienced during my time in graduate school and at Texas A&M in general. When I have wandered, He has remained faithful. He has continually led me to the right place and the right people at the right time. He has gifted me with talents and abilities that have helped me achieve more than I could have imagined. "My flesh and my heart may fail, but God is the strength of my heart and my portion forever" (Psalm 73:26).

# CONTRIBUTORS AND FUNDING SOURCES

This work was supported by a dissertation committee consisting of Professors Alex Thomasson, co-advisor, and Yufeng Ge of the Department of Biological and Agricultural Engineering, and Professor Cristine Morgan, co-advisor, of the Department of Soil and Crop Science.

Data collection and graduate research assistantship funding was provided by the USDA NRCS Soil Survey in Texas.

# TABLE OF CONTENTS

Page

# LIST OF FIGURES

Page

# LIST OF TABLES

Page

# 1. INTRODUCTION AND LITERATURE REVIEW

## 1.1. Introduction

The Columbia Bottomlands ecosystem, though highly valuable in terms of wetlands, wildlife, and biodiversity, loses thousands of acres yearly to urbanization, agriculture, and other anthropogenic activities (U.S. Fish & Wildlife Service, 2013). While Section 404 of the Clean Water Act (Public Law 92-500, 33 U.S. Congress 1251) places wetlands under the jurisdiction of the United States Army Corps of Engineers (USACOE), failure to identify much of the Columbia Bottomlands as jurisdictional wetlands is believed to contribute heavily to deforestation and draining (Miller and Bragg, 2007). The unique characteristics of Vertisols, soils that underlay much of this area, often obscure traditional markers of wetland soils, resulting in misidentification and, ultimately, habitat loss (Miller and Bragg, 2007). Improving or developing new methods of identifying and monitoring soil moisture and saturation in Vertisols could facilitate more accurate delineation of jurisdictional wetlands, protecting parts of the Columbia Bottomlands from further habitat loss. Electrical Resistivity Tomography (ERT), has been proposed as a possible method for non-invasive, temporal monitoring of soil moisture in Vertisols.

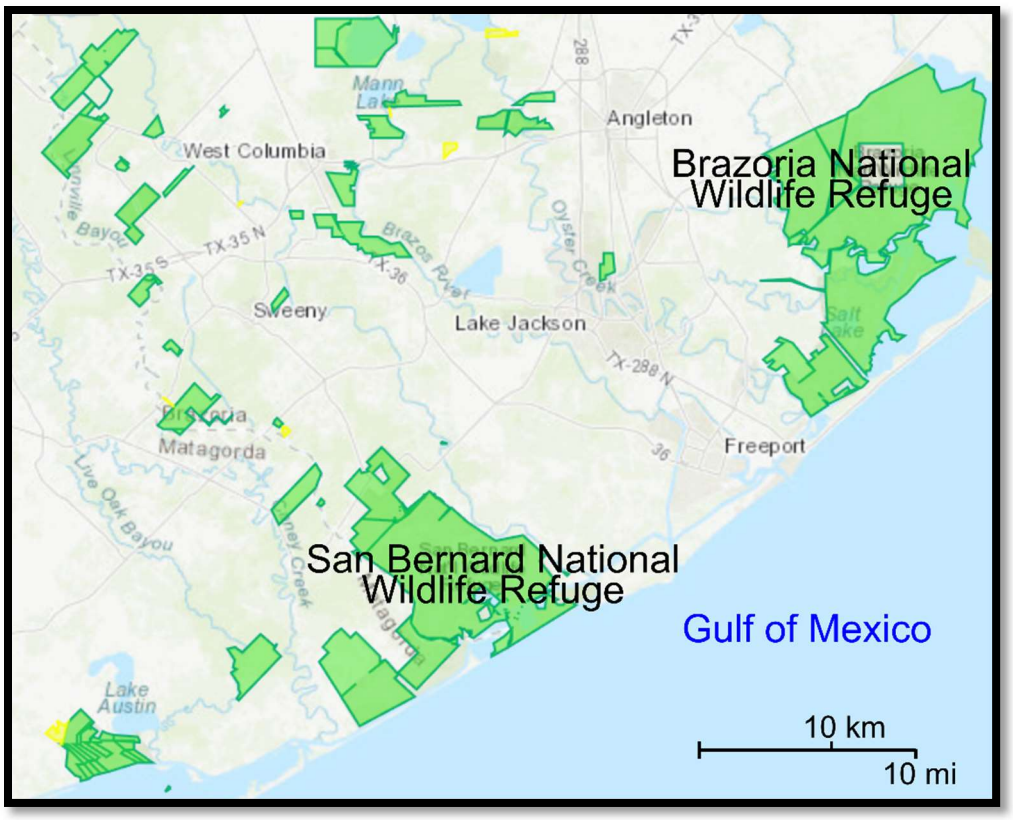


Figure 1: San Bernard and Brazoria National Wildlife Refuges (adapted from U.S. Fish & Wildlife Service, 2018).

The Columbia Bottomlands ecosystem, located in the Texas Gulf Prairie, spans Brazoria, Fort Bend, Matagorda, and Wharton Counties. The floodplains of the lower Brazos, San Bernard, and Colorado Rivers combine in this area. The bottomland hardwood forests that comprise much of this ecosystem are "extremely diverse and productive habitats," serving as seasonal or year-round homes to migratory birds, waterfowl, and even bald eagles, among others (U.S. Fish & Wildlife Service, 2013). Estimated at 2,400 square miles by settlers in the 1830s, the forests were cut down to less than half that by 1900, leaving roughly 700,000 acres. Presently only around

150,000 acres remain (U.S. Fish & Wildlife Service, 2013). Though the forests are not cleared for their timber, which is low in commercial value, the lands they occupy are continually cleared for grazing and agricultural production, residential development, urbanization, and infrastructure expansion. The United States Fish and Wildlife Service (USFWS) currently protects a remnant of this ecosystem under the San Bernard and Brazoria National Wildlife Refuges (Figure 1) and has developed plans to purchase 42,000 acres of privately-owned territory within the Columbia Bottomlands. This would expand the size of these refuges to 70,000 acres — 10% of the land covered by forests in 1900 (U.S. Fish & Wildlife Service, 2013). Further preservation and restoration of this invaluable ecosystem could be accomplished if the forests were identified as jurisdictional wetlands under the Clean Water Act. Though many of the markers of wetlands are present in the Columbia Bottomlands, the unique characteristics of the underlying soils of much of the region make it easy to overlook wetland criteria, contributing to the unwarranted exclusion of acres of wetlands from jurisdictional classification (Miller and Bragg, 2007).

Wetlands subject to the jurisdiction of the USACOE under Section 404 of the Clean Water Act are defined as:

> *"those areas that are inundated or saturated by surface or ground water at a frequency and duration sufficient to support, and that under normal circumstances do support, a prevalence of vegetation typically adapted for life in saturated soil conditions. Wetlands generally include*

> *swamps, marshes, bogs and similar areas"* (33 CFR 328.3, quoted in Mausbach and Parker, 2001).

In order to be classified as a wetland, a given area must contain appropriate indicators in the categories of hydrophytic vegetation, hydric soil, and wetland hydrology, all of which are described in detail in the *Regional Supplement to the Corps of Engineers Wetland Delineation Manual: Atlantic and Gulf Coastal Plain Region* (USACOE, 2010). The handbook includes a discussion of "difficult wetland situations in the Atlantic and Gulf Coastal Region," with a section on "problematic hydric soils" that refers to the very soils that underlay much of the Columbia Bottomlands: "slightly to strongly alkaline bottomland-hardwood Vertisols in Texas" (USACOE, 2010). An extensive six-year, multiagency study, conducted across Vertisols in the Columbia Bottomlands, yielded evidence that much of the Columbia Bottomlands should be classified as wetlands, though the unique characteristics of Vertisols present significant difficulty in accurately classifying many areas as such (Jacob et al., 1997; Miller and Bragg, 2007).

Vertisols are a soil class defined as having clay content greater than 30%, exhibiting shrink-swell characteristics that can require specialized agricultural practices, and, often, marked by unique surface and subsurface features (Amidu and Dunbar, 2007). Shrink-swell behavior is the result of moisture-dependent volume change as the smectitic clay minerals typical of Vertisols dry out and rewet (Miller and Bragg, 2007). Surface features that result from this behavior include microrelief structures known as gilgai — microhighs and microlows, also called depressions and mounds, separated by

microslopes (Figure 2). A mound and its neighboring depression may be as much as 2 to 5 m apart, with a peak-to-trough elevation change of 0.02 to 0.05 m (Miller and Bragg, 2007).

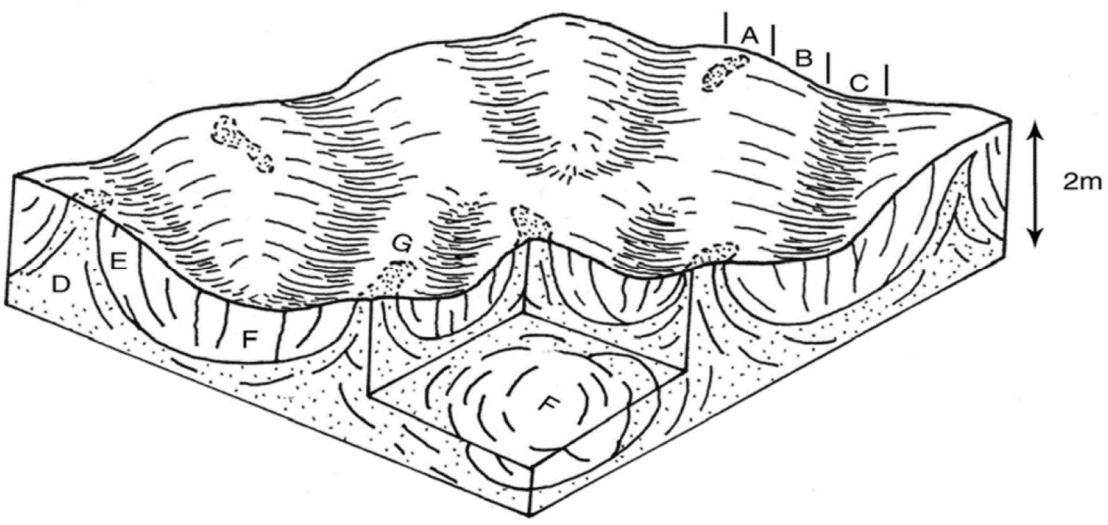


Figure 2: Surface and subsurface features of a Vertisol: A) Microhigh, B) Microslope, C) Microlow, D) Chimney, E) Intermediate, F) Bowl, G) Puff (Miller and Bragg, 2007).

Subsurface features such as bowl and chimney formations are associated with each type of surface feature. A microlow is typically underlain by a bowl — an area of soil from the upper layers of the profile that is bowl-shaped and bounded by slickensides. Chimneys are associated with microhighs and consist of materials from lower layers of the profile that are pushed upward with time as the soil expands and contracts. Because the chimney material comes from lower layers, this soil tends to be lower in organic matter content than that in a bowl formation, lighter in color, and more

alkaline, and often contains nodules of calcium carbonate (Miller and Bragg, 2007). The striking difference in appearance between bowl and chimney features is evident in Figure 3. If a chimney reaches the top of the soil profile and is exposed on the surface, the feature is called a puff. Microslopes are associated with transition zones between the bowl and chimney features (Miller and Bragg, 2007).

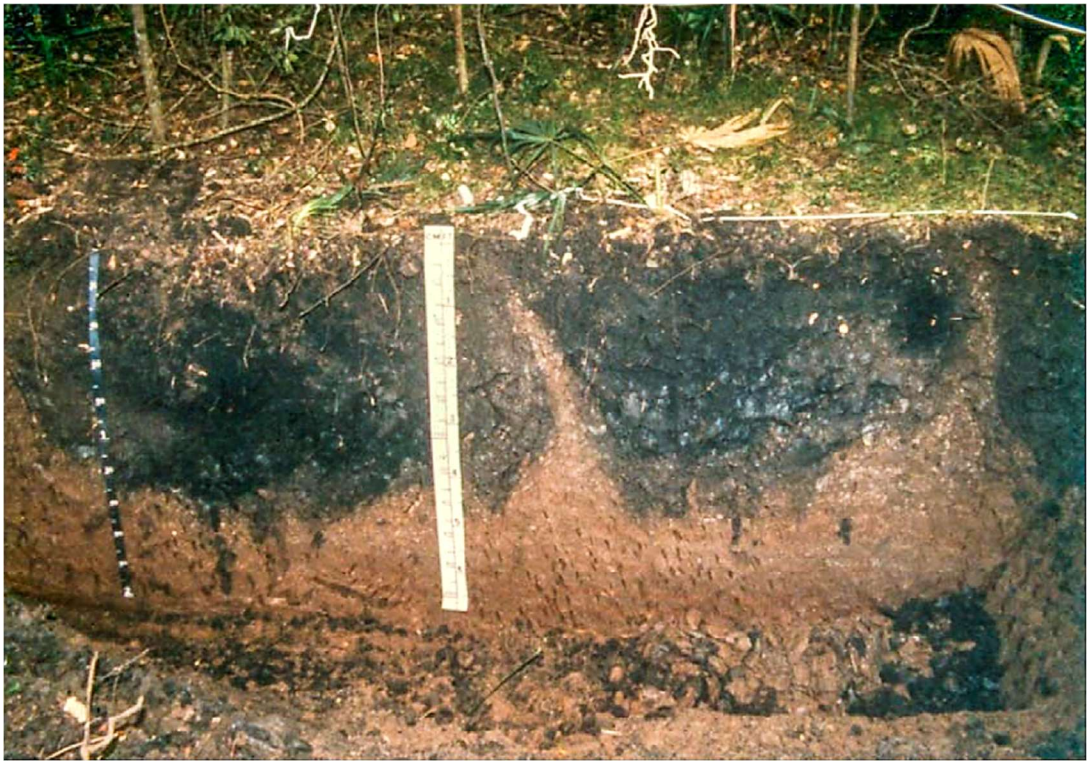

Figure 3: Bowl and chimney formation typical of Vertisol soils (adapted from Miller and Bragg, 2007).

In addition to the surface and subsurface features described above, the shrink-swell behavior typical of Vertisols also produces significant cracking throughout the soil

profile during prolonged periods of low soil moisture conditions. The combined effect of these unique characteristics influences soil moisture content and water flow, often producing preferential flow paths that encourage saturation in some areas but not others (Amidu and Dunbar, 2007). Such flow paths may extend unseen throughout the clay layer, sometimes producing perched water tables. Determining whether a given Vertisol wets via endosaturation, when the soil is saturated by a rising water table, or episaturation, when a perched water table forms as surface water infiltrates the soil surface and collects on a layer of relative impermeability, is greatly complicated by these unusual hydrologic behaviors.

The shrink-swell behavior of Vertisols and the preferential flow paths they often produce also interfere with the development of hydric soil indicators commonly expected to appear in wetland soils (Jacob et al., 1997). This interference takes two forms: seasonally-ponded soils that develop perched water tables (USACOE, 2010), and incomplete saturation of the soil matrix due to runoff (Miller and Bragg, 2007). In the first instance, precipitation travels down preferential flow paths and perches on top of a clay pan near the surface. The clay pan limits the depth to which the soil may saturate, restricting the development of hydric soil indicators (USACOE, 2010). In the second instance, soil cracks absorb water during precipitation events, causing the surrounding soil to swell. As the soil swells, the cracked surface is sealed off, causing remaining surface water to run off into lower-lying areas. Since the soil matrix is unable to saturate due to runoff and surface sealing, the development of hydric soil indicators is again inhibited, even though the area exhibits the flooding and ponding behavior characteristic

of wetlands (Miller and Bragg, 2007). As noted in the *Wetland Delineation Manual*, the Vertisols underlying the Columbia Bottomlands are alkaline (USACOE, 2010). Miller and Bragg (2007) assert that alkaline soil conditions interfere with the development of hydric soil indicators such as redoximorphic features. Additionally, the red parent material from which these Vertisols derive may obfuscate changes in soil color usually associated with iron reduction. Inhibition or masking of typical redoximorphic features, rather than lack of appropriate conditions, may preclude proper classification of hydric soils and, therefore, designation of the Columbia Bottomlands as protected wetlands.

The National Technical Committee for Hydric Soils (NTCHS) defines hydric soils as those "formed under conditions of saturation, flooding, or ponding long enough during the growing season to develop anaerobic conditions in the upper part" (Soil Survey Staff, 1999; quoted in Mausbach and Parker, 2001). Wetlands have a 50% probability of saturation or flooding during the growing season of any given year. In undisturbed wetlands, typical indicators of these conditions include the presence of surface water, high water tables (within 30 cm of the soil surface) including perched water tables, and saturated soil within 30 cm of the soil surface (USACOE, 2010). The presence of saturated soil, perched water tables, or high water tables as indicators of hydric soil-forming conditions may be detected and monitored by instruments that measure soil moisture, obviating the presence of typical markers to classify the soil as hydric. However, invasive methods of soil moisture measurement, such as piezometers and tensiometers, are destructive, making data collection at a given point unrepeatable, and measure soil moisture only at unique spatial points (Amidu and Dunbar, 2007).

Additionally, the shrink-swell nature of Vertisols is thought to interfere with the performance of tensiometers because the soil pulls away from the instrument as it dries, potentially disrupting the seal necessary for accurate measurements (Allen et al., 2005). If soil shrinkage is sufficient to disrupt tensiometer operation, preferential flow paths could also develop as soil shrinks away from installed measurement devices, allowing water to travel via bypass flow and collect in bore holes. Resulting increases in soil moisture at the point of measurement could artificially inflate moisture measurements. Accordingly, noninvasive methods of moisture measurement are desirable since they neither alter soil structure nor create preferential flow paths that invalidate soil moisture measurements (Amidu and Dunbar, 2007).

One noninvasive method that merits consideration for detection of saturated conditions in Vertisols is the use of Electrical Resistivity Tomography (ERT) to measure soil resistivity (ohm-m) as a proxy for soil moisture. In this method, a switchbox connected to a series of electrodes (Figure 4) is used to pass electricity at a known current through the soil to various depths and ranges of soil volume to develop a map of soil resistivities in the measured area. This map creates a visual representation of subsurface features and may also be called a survey or transect (Figure 5). The volumes and depths measured in a survey depend on electrode spacing, the distance between any two consecutive electrodes, and the electrode configuration used by the ERT instrument to conduct measurements (Dahlin, 2001; Everett, 2013a; Zhou et al., 2000). Different electrode configurations or arrays may be selected based on their properties and the goals of a given survey. The four-electrode Wenner array (Wenner, 1915) is thought to

be best suited for use in near-surface groundwater tables because it best detects vertical variations in resistivity and provides approximately consistent measurement spacing with depth, maintaining measurement resolution throughout the targeted depth (Amidu and Dunbar, 2007). Additionally, this configuration is often least-subject to noise contamination and performs well with depth (Dahlin and Zhou, 2004; Everett, 2013a).

Figure 4: Left) A SuperSting R8 Earth Resistivity/IP Meter switchbox connected to a line of electrodes through yellow electrical cables. Right) Metal stakes serve as electrodes

and are connected to metal contacts in the electrical cables directly or through smaller cables with electrode clips.

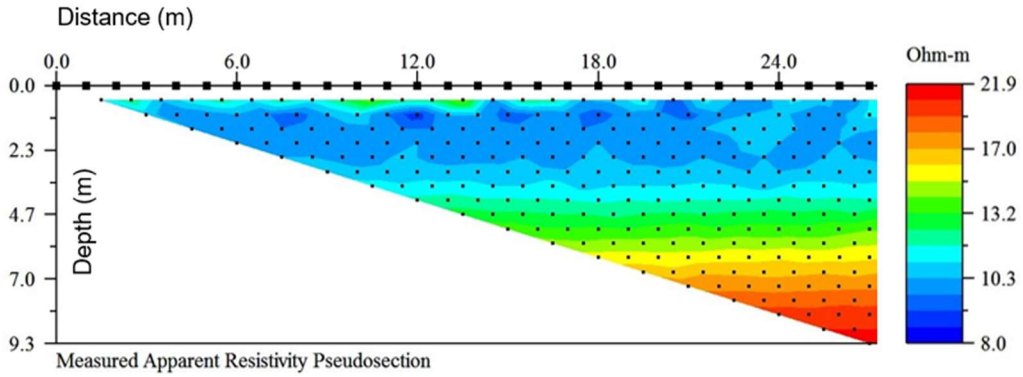


Figure 5: A partial example of a resistivity transect constructed using ERT. Points denoted by black dots represent pseudolocations of resistivity measurements. Color scale represents soil resistivity interpolated between pseudolocations.

During ERT surveys, the switchbox cues two electrodes per resistivity measurement to emit current, and two electrodes to detect voltage or potential (Advanced Geosciences, 2006; Everett, 2013a). For a Wenner array, the electrodes that measure potential, **P** and **Q**, are placed between the current-injecting electrodes, **A** and **B**. Electrode combinations **A** and **P**, **P** and **Q**, and **Q** and **B** are all equally separated by a distance of $n \cdot a$, where $n$ is a positive-integer multiplier of the electrode spacing, $a$ (m). Figure 6 illustrates the configuration for the first measurement collected using a Wenner array, $\rho_{a,1}$, when $n = 1$. While the measurement taken encompasses a volume of soil beneath the array, a pseudolocation is assigned to represent the measured area. The pseudolocation of $\rho_{a,1}$ will fall at the center of the configuration at a depth of $0.5n \cdot a$. The top line of measurements in a survey is constructed as the switchbox activates

subsequent electrodes such that $\mathbf{P_1}$ becomes $\mathbf{A_2}$ for measurement $\rho_{a,2}$, $\mathbf{Q_1}$ becomes $\mathbf{A_3}$ for $\rho_{a,3}$, etc., as demonstrated in Figure 7. Deeper lines are constructed as $n$ increases and the process repeats (Figure 8). Surveys that use more electrodes at a wider base electrode spacing produce deeper measurements, but sacrifice resolution (Zhou et al., 2000).

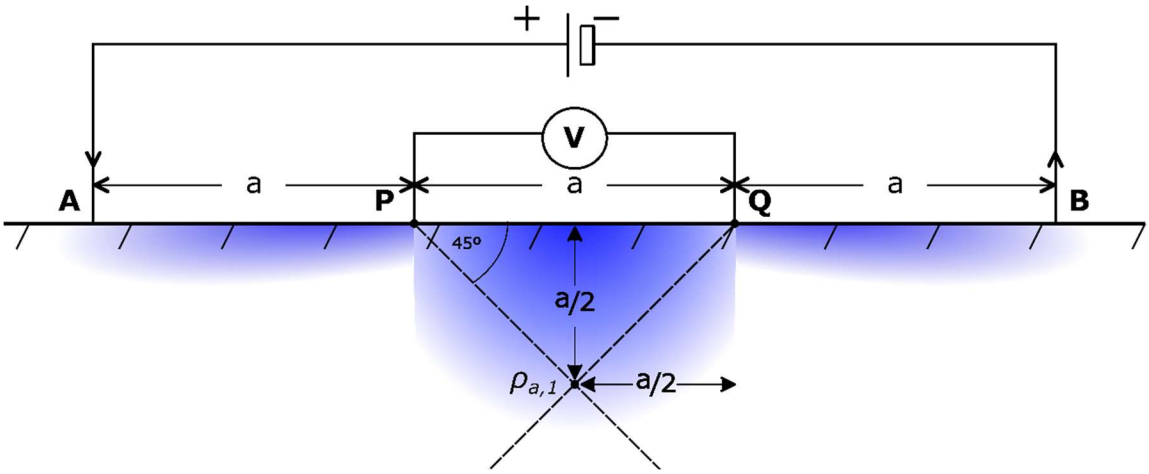


Figure 6: Wenner array electrode configuration with pseudolocation and approximate senstivity map of resulting measurement at base electrode spacing (adapted from Everett, 2013a).

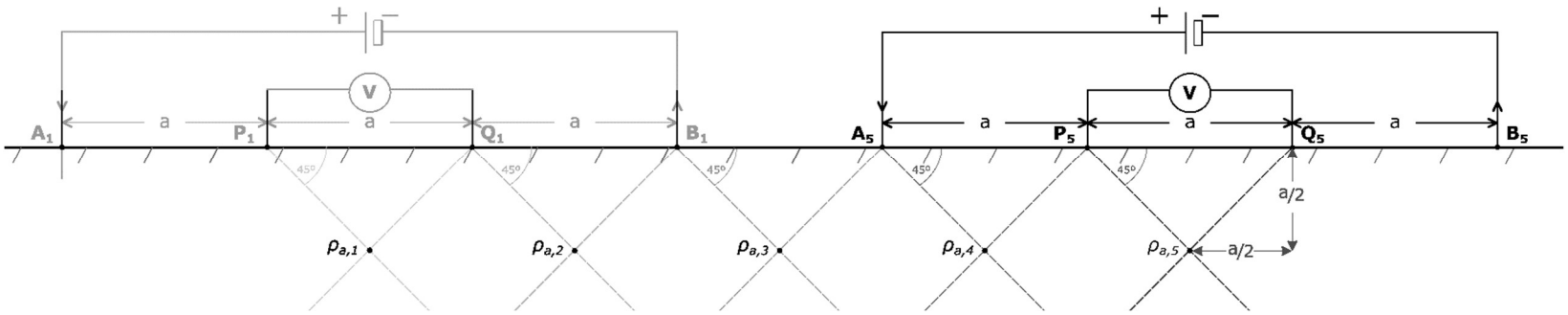


Figure 7: Example of Wenner array electrode configuration demonstrating progression through five linear measurements, and pseudolocations of resulting measurements at base electrode spacing.

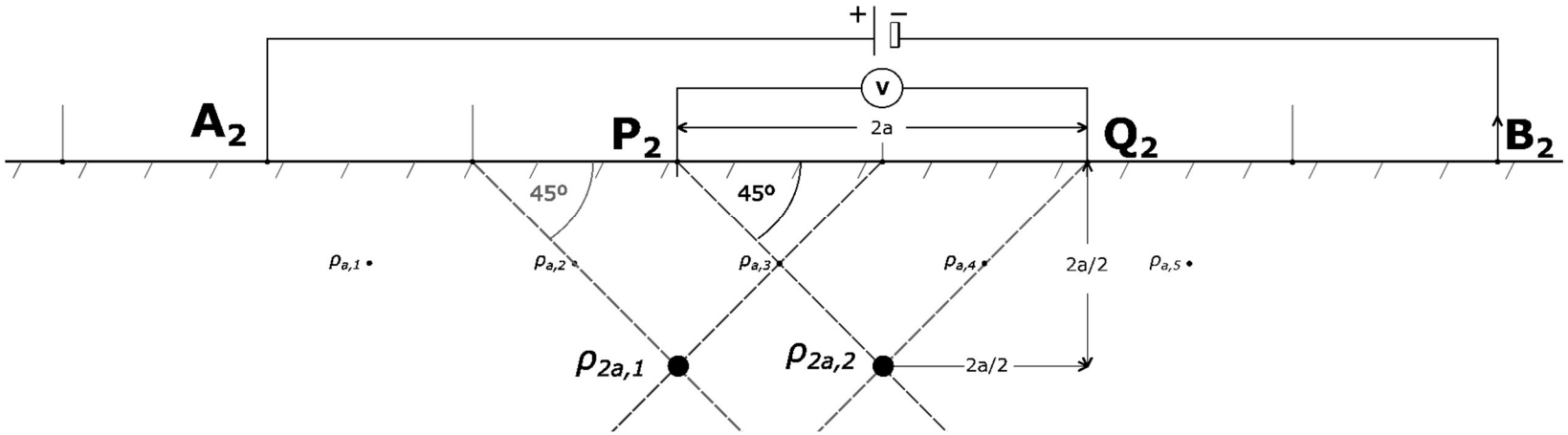


Figure 8: Example of Wenner array electrode configuration demonstrating progression into a deeper row of measurements, and pseudolocations of resulting measurements at twice the base electrode spacing.

With a known injected current, $I$ (amps), and voltage, $V$ (volts), measured by the ERT instrument, the bulk electrical resistivity of the soil, $\rho_{a,}$, is calculated by

$$\rho_a = \kappa \frac{V}{I}, \qquad \textit{Equation 1}$$

where $\kappa$ is the geometric factor matching the electrode configuration. For the Wenner array, $\kappa = 2\pi a$ (Everett, 2013a).

The resistivity data collected by the ERT instrument, using the Wenner configuration, represent volumetric weighted-average resistivities within three-dimensional subsections of soil (Figure 6), rather than the true resistivity at a given point in the soil profile (Zhou et al., 2000). This measurement is known as apparent resistivity and has units of ohm-m. Further, this process results in the indirect measurement of subsurface information — apparent electrical resistivity at various depths — from the Earth's surface (Everett, 2013b). A process known as inversion is used to extract the desired information from these indirect, weighted-average measurements. True resistivity is estimated from apparent resistivity to create a more accurate "picture" of subsurface characteristics that indicate changes in soil texture, salinity, or water content. In one part of this process, called forward modeling, any prior knowledge available about the subsurface characteristics of the measurement site are used to construct an initial model of the site. Applying this model produces a theoretical data set that represents what the ERT data would look like if the model were correct. This synthetic data set is then compared to the data collected by the ERT instrument to improve upon the theoretical model. Based on the comparison of the two data sets, a new forward

model is constructed which produces a new synthetic data set to be compared to the measured apparent resistivity data. This iterative process continues until the model that most closely agrees with the apparent resistivity data is identified, though the solution is non-unique (Constable et al., 1987). The final model is thought to represent a simplified picture of the subsurface resistivity of the measurement site (Everett, 2013a). Abrupt changes in the subsurface, such as boundaries between bedrock and fine soil deposits, are not distinguishable using such models because the resistivity data are volume-averaged (Zhou et al., 2000).

Since resistivity is related to soil moisture, texture, and salinity (Archie, 1942), the final model selected by the inversion process should provide an idea of the soil moisture content along the measured soil profile if salinity and texture are homogenous. In soils that violate the assumption of homogeneity, textural horizons also appear in ERT data (Zhou et al., 2000). In such cases, resistivity will likely vary more between soil layers than between regions of high and low moisture, making determination of soil moisture unlikely, if not impossible, without knowledge of the soil profile. While the resistivity of a clay layer may range from 5 ohm-m in a wet clay to 20 ohm-m in a very dry clay, moist sand can reach 200 ohm-m, and shale can reach 500 ohm-m (Everett, 2013a).

Collecting profile information such as soil texture may improve understanding of resistivity data by indicating where textural changes influence resistivity at a given site. Such information can be gathered from soil cores, with textural data gleaned from particle size analysis (PSA). Visible and near-infrared (Vis/NIR) diffuse reflectance

spectroscopy readings from dried, intact soil cores may be used to predict clay content as a proxy for soil texture, improving resistivity models and prediction of soil moisture content while circumventing the costly, laborious process of grinding and performing PSA on hundreds of soil samples (Waiser et al., 2007).

ERT has been shown to non-invasively enable spatial and temporal characterization of soil moisture for various soil types (Michot et al., 2003), making it worthwhile to investigate ERT's ability to detect and monitor soil moisture in Vertisols. Amidu and Dunbar (2007) have used ERT to identify preferential flow paths and detect soil moisture levels in a Texas Vertisol, noting that, at high soil moisture levels, large changes in soil moisture produce only very small changes in soil resistivity. This relationship warrants investigation into the ability to distinguish very slight soil moisture changes in nearly-saturated Vertisols using ERT.

### 1.2. Literature Review

The conventional method of directly measuring soil moisture involves excavating, weighing, drying, and reweighing soil samples to calculate the weight of the water evaporated relative to the total weight of the sample. This method is not only destructive, but expensive in terms of time, labor, and energy. Less intensive processes are inherently more practical if proven to be effective. Indirect and less destructive methods of measuring or estimating soil moisture are available: tensiometers and piezometers work well in wet-to-moist soils but do not work well long-term in high-clay soils. Heaving of the soil through wetting and drying cycles disrupts the performance of

such instruments and installation holes can serve as paths for preferential water flow (Miller and Bragg, 2007). Neutron moisture meters work well for monitoring soil moisture, especially in Vertisols (Chanasyk and Naeth, 1996; Dinka et al., 2013; Neely et al., 2014). However, an access hole is still needed and permitting for storage and travel with a radiation source can be cumbersome. Volumetric water content can also be estimated based on a soil's dielectric properties measured by capacitance sensors or time-domain reflectometry probes, but such methods have limited accuracy in Vertisols (Evett et al., 2006, 2003). All of these methods, though effective with appropriate application, require somewhat destructive installation, are limited in spatial extent, and yield only discrete measurements.

If applicable, ERT is an attractive method for measuring and monitoring soil moisture in Vertisols and other soils because of its non-invasive setup and the spatial extent and resolution at which measurements can be made. For example, a single 56-electrode survey with a 1-m electrode spacing could sound to a maximum depth of 28 m. An ERT survey could be designed to span nearly any depth and distance by changing the number and spacing of electrodes.

Amidu and Dunbar (2007) used ERT to study seasonal wetting and drying characteristics of the upper 1.4 m of a Texas Vertisol. Volumetric soil moisture contents ranging from approximately 0.1 to 0.8 $m^3 m^{-3}$ were identified non-invasively using electrical-resistivity measurements of 0 to 100 ohm-m. Resistivity data were collected using a Sting R1/Swift resistivity system (Advanced Geosciences, 2006). A total of 32 profiles were measured from 1 May 2005 to 22 April 2006 using roll-along dipole-dipole

and Schlumberger arrays with an electrode spacing of 0.5 m. The apparent resistivity data collected by the Sting system were temperature-corrected using the lab calibration method recorded by Rein et al. (2004) and inverted using RES2DINV (Loke and Barker, 1996) to construct a subsurface resistivity model of the site. The apparent resistivity data were calibrated to soil moisture using soil samples collected from the research site. Resistivity for the samples was measured with the Sting system, and conductivity and water temperature with a YSI model 30 conductivity meter (YSI, Yellow Springs, OH). Data were temperature-corrected and used to fit a model that expresses true resistivity as a function of apparent resistivity. A relationship between soil resistivity and soil moisture was then fitted from a modified version of the power-law relation (Yeh et al., 2002). The authors were able to establish that apparent resistivity data can be used to characterize seasonal wetting and drying in the targeted Vertisol. The authors further noted that under high soil moisture conditions, above 0.5 $m^3$ $m^{-3}$ volumetric water content, large changes in soil moisture resulted in small changes in apparent resistivity. Under low soil moisture conditions, below 0.18 $m^3$ $m^{-3}$, even small changes in soil moisture resulted in large changes in apparent resistivity. The upper 0.5-m soil layer was found to be most affected by seasonal weather patterns, while the middle 0.5 to 1.1-m layer was found to maintain the highest water content throughout the year, regardless of fluctuations in weather. The authors were able to detect the presence of preferential flow paths that affected soil moisture conditions in the test site using the ERT measurements. Apparent resistivity did not facilitate independent quantification of soil moisture content, but reflected relative differences in soil moisture that could be calibrated using

laboratory data. The authors fitted a curve to soil moisture and resistivity data with RMSE of 6.18%.

Michot et al. (2003) applied ERT to an irrigated corn crop in Beauce, France, in an effort to nondestructively measure the flow of water through a loamy-clay Calcisol with time. The study concluded that soil water content could be determined using ERT when calibrated according to soil moisture-resistivity relationships by soil horizon. An attempt to calibrate volumetric water content with resistivity in-lab with soil cores collected from the study site demonstrated that the resistivity of the soil cores changed with core diameter. Accordingly, the field relationship between soil moisture and resistivity was developed by extracting soil by layer, inserting electrodes, TDR probes, and temperature sensors into each layer, perpendicular to the soil surface exposed by the excavation, and refilling the pit by soil layer with the excavated soil. Resistivity, soil temperature, and moisture content data were collected with this setup over the course of a year. The resulting temperature-corrected field calibration enabled the authors to estimate volumetric soil moisture from ERT resistivity data with an RMSE of 0.036 $m^3$ $m^{-3}$ in the plow layer. This study also detected the presence of preferential flow patterns in high-clay soils. The authors concluded that traditional invasive sampling methods for soil moisture estimation are insufficient in representing the more complex realities of soil moisture and do not allow for temporal monitoring. ERT estimations of water content were shown to be significant, though such results are not necessarily replicable in different soil types.

Zhou et al. (2000) used ERT to measure the depth to limestone bedrock in a clay soil approximately 9-m thick. A dipole-dipole electrode configuration with an electrode spacing of 3 m was used in 2D transects ranging from 81 to 249 m in length, and the data were inverted using RES2DINV (Loke and Barker, 1996). The authors noted that, despite abrupt transitions from clay to limestone, which should correspond to abrupt changes in resistivity, the images produced by the inverted models do not identify the exact depth to the bedrock, but instead show a transitional region that may span several meters. The authors attempted to correct for this using "ground-truth" data collected from soil borings along each transect when interpreting the inversion output. The difference between depth-to-bedrock measured in the soil borings and from ERT data averaged 2.4 m with a maximum difference of 10 m overall. These discrepancies were attributed to a number of potential causes, including: environmental factors that interfered with data quality, the volume-averaging nature of resistivity that often overlooks small-scale variations in the subsurface, the inherent non-uniqueness of the inversion process, potential inaccuracies in ground-truth data, and the inability of 2D-modeling to accurately characterize 3D geologic formations.

Ackerson et al. (2014) used lab-based electrical resistivity and soil water content measurements from drying soil clods to develop an empirical model that predicted electrical resistivity from volumetric water content with an RMSE of 8.3 ohm-m and $r^2$ = 0.84. The model was used to predict soil electrical resistivity in a Texas Vertisol with in-situ soil moisture content data collected using a neutron soil moisture meter. In-situ electrical resistivity data were collected with a SuperSting R8-IP Resistivity meter using

a 3D dipole-dipole array at a base electrode spacing of 0.5 m. The ERT data were inverted with EarthImager3D (Advanced Geosciences, 2008) and compared to the electrical resistivity values predicted by the empirical model. In the absence of soil cracks, measured electrical resistivity agreed with the empirical model. The presence of soil cracks was found to influence soil resistivity beyond expected changes resulting from decreased water content, with the average measured electrical resistivity exceeding predicted values by over 15,000 ohm-m within the depth range of 0.2 to 0.8 m. The authors further found that the low sensitivity and high noise of ERT data made estimation of water content from field measurements of soil electrical resistivity impossible. Further work by the authors (Ackerson et al., 2017) did demonstrate that ERT was useful in identifying the spatial structure of cracking networks in the same field experiment.

Jayawickreme et al. (2008) collected 27 resistivity data sets from October 2006 to September 2007 using permanently-installed electrodes and a Wenner array. The study site was partially mature Maple forest and partially grassland. For each land type, one location within the transect was outfitted with capacitance-type soil moisture loggers at two depths (20 and 80 cm) and temperature arrays at seven depths ranging from 5 to 147 cm. A differential inversion algorithm developed by LaBrecque and Yang (2001) was used to establish a baseline resistivity distribution and determine the resistivity change over a given time period. Temperature data from the two vertical sensor arrays were interpolated and used to correct inverted resistivity data for variations in soil temperature according to methods described in Hayley et al. (2007). Archie's power

function (1942) was fitted to the temperature-corrected resistivity data and water contents from the two soil moisture loggers with an $r^2$ value of 0.92 and p-value below 0.0001. Equation parameters for sand and clay loam were used based on the soil texture of the site.

Cardenas and Kanarek (2014) conducted monthly resistivity surveys in sand and loamy sand underlaying an isolated region of loblolly pines in Bastrop State Park, Texas. Data from the 165-m long transect (3 m electrode spacing) were inverted using RES2DINV (Loke and Barker, 1996). Changes in soil electrical resitivity due to temperature variations, calculated according to Hayley et al. (2007), ranged from -12.7% to +8.3%. Soil moisture was calculated from estimates of electrical permittivity collected at four locations and six depths per location using Delta-T Devices handheld ThetaProbe ML2x and PR2 profile probes. A linear regression model was developed to predict soil moisture from log resistiivty with an $r^2$ value of 0.70. Changes in resistivity over time were determined by inverting each data set individually and comparing data from different dates (Miller et al., 2008). Given a RMSE of less than 5% for each inverted data set and expected resistivity changes due to temperature of 10% or less, the authors concluded that only temporal resistivity changes greater than 10% could be reliably understood to result from changes in soil moisture.

### 1.3. Objectives

The purpose of this research was to determine, in Vertisols: 1) whether log resistivity is a significant predictor of volumetric water content, 2) whether ERT data

can better predict water content than can clay content, 3) whether prediction models for water content are site-specific based on the significance of slopes and intercepts in dummy variable regression and ANCOVA, and 4) whether ERT is suitable for monitoring soil moisture conditions over time, as determined by whether regression models for change in water content and change in log resistivity over time are significant, and whether the slopes of the models for different locations are significantly different from each other.

# 2. MATERIALS AND METHODS

## 2.1. Overview

This research focused on two Vertisols in Texas: initial exploration took place at the Brazos River Site (BRS) on the Texas A&M Research Farm west of College Station; a follow-up study was conducted at the Dance Bayou Wildlife Area (DB), part of the San Bernard National Wildlife Refuge in Brazoria County (Figure 9). At both sites, ERT research was conducted with a SuperSting R8-IP Resistivity meter (Advanced Geosciences, 2006), commonly referred to as a SuperSting (Figure 4, left). The SuperSting was used to measure apparent soil resistivity during the seasonal wetting period. Soil cores at each test site were collected and analyzed to validate the soil texture and moisture content of each location. Reflectance readings in the 350 to 2500-nm wavelength range were collected from a subset of cores using an Agri-Spec Vis/NIR reflectance spectroscopy unit (Analytical Spectral Devices Inc., Boulder, CO). Vis/NIR data were used to predict percent clay content in soil samples as a proxy for soil texture. Data analysis focused on the relationships between clay content, soil moisture, and inverted resistivity values to evaluate the suitability of applying ERT methods to determine soil moisture conditions in suspected wetland Vertisols.


Figure 9: Locations of Brazos River and Dance Bayou study sites (Satellite imagery from Google Earth).

## 2.2. Brazos River Site

Initial equipment calibration and model development were conducted on a Vertisol at the BRS, which has a well-documented soil profile constructed from drilling logs for a series of well-nests overlaying the site (Figure 10). The thickness (depth) of the surficial Ships clay soil (very fine, mixed, active, thermic Chromic Hapludert)

increases moving north and east. While the depth-of-clay is similar for the westernmost wells, C1-C3, at approximately 5 m (Table 1), the wells closest to the river range in depth-of-clay from 7 m at A1 to 9 m at A3.

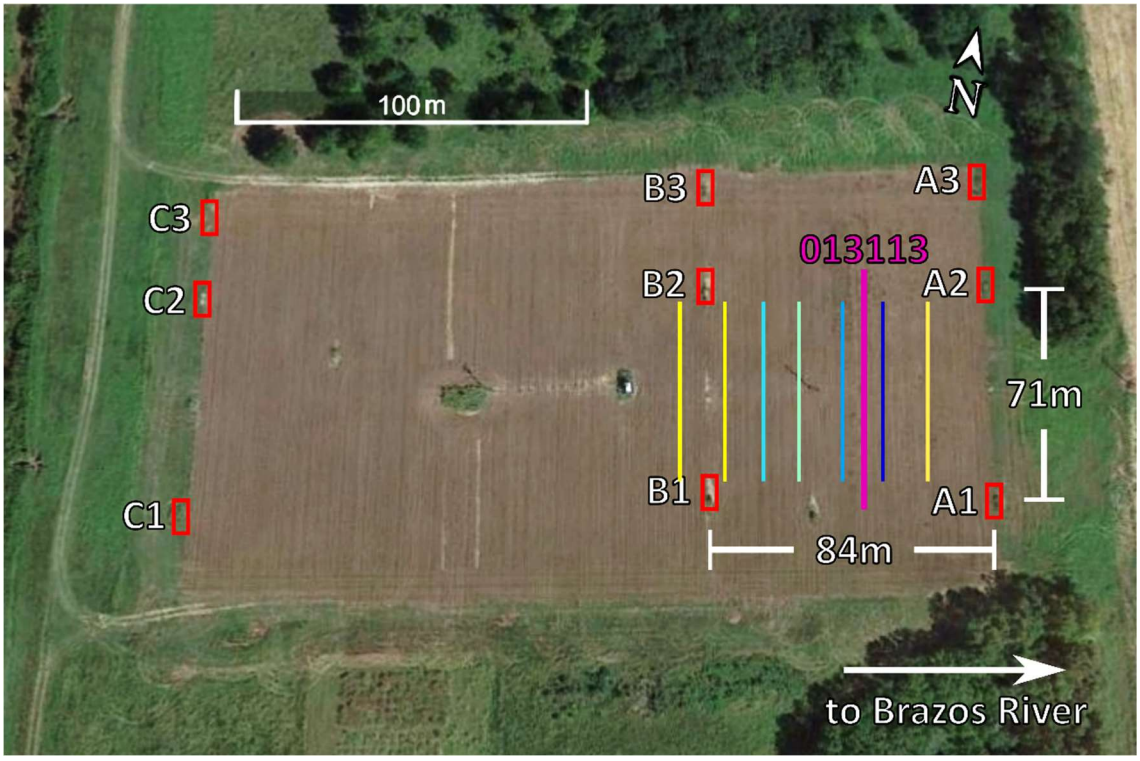


Figure 10: Map of Brazos River Site denoting well locations and approximate lengths and locations of resistivity transects (Satellite imagery from Google Earth).

Table 1: Approximate depths of clay layer, in m, by well site (Munster et al., 1996).

| | A | B | C |
|---|---|---|---|
| **1** | 7 | 6 | 5 |
| **2** | 8 | -- | 5 |
| **3** | 9 | 7 | 5 |

The Ships clay is underlain by unconsolidated alluvium consisting of fine sand nearest the bottom of the clay (Figure 11). Particle size increases, with depth, to gravel before the profile transitions to the Yegua Shale formation. The water table, a 350-mile minor aquifer along the Brazos River (Ashworth and Hopkins, 1995; George et al., 2011), lies in the alluvial deposit beneath the clay layer (Munster et al., 1996; Shah et al., 2007; Wrobleski, 1996). A preliminary ERT measurement conducted 31 January 2013 ran parallel to the river with an electrode spacing of 1.5 m (Figure 10). This transect was 81.5 m long and measured to an approximate depth of 11.1 m. Two soil cores were pulled for this survey: one at 38.5 m from the origin of the survey, and a second at 50 m from the origin. The cores reached depths of 4.82 and 3.5 m, respectively.

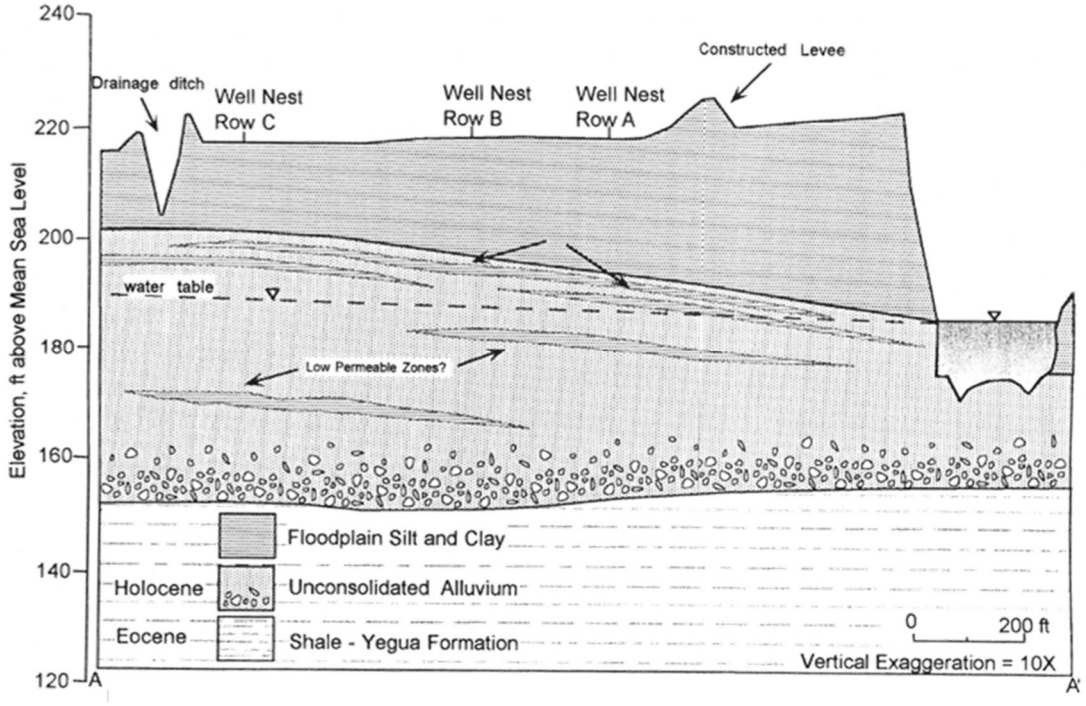


Figure 11: Geologic cross-section of the Brazos River Site (Wrobleski, 1996).

Subsequent ERT measurements were conducted in April of 2013 using a Wenner electrode array with 1-m spacing (Figure 12). These transects measured 56 m in length and approximately 10.3 m in depth to capture the transition region between clay and fine sand in the soil profile. Seven such transects were collected running parallel to the river with all starting locations on the same axis running perpendicular to the river. Each survey was conducted at a different perpendicular distance from the river (Figure 10) because of the destructive nature of soil coring and the likelihood that boreholes would interfere with the path traveled through the soil by the electrical current, creating noisy data. Where possible, soil cores were pulled until the transition layer between clay and

fine sand was reached. The process of collecting soil cores is discussed in more detail in Section 2.5.

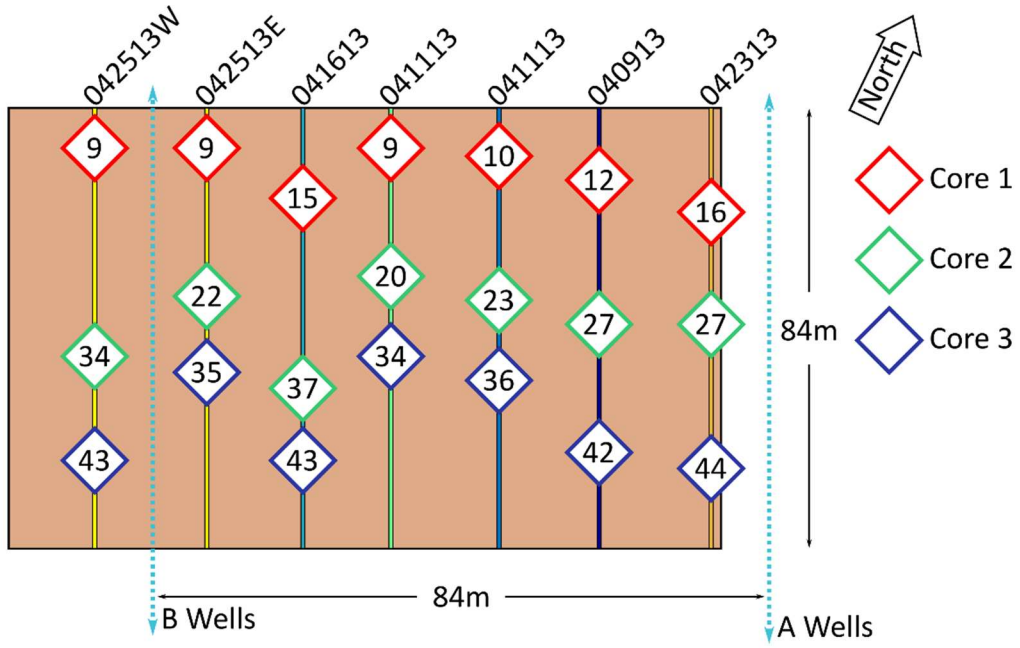


Figure 12: Approximate locations of Brazos River Site transects and cores collected in April 2013.

## 2.3. Dance Bayou Site

A second research site was selected from a NRCS benchmark soil at the Dance Bayou Wildlife Area in Brazoria County, Texas (Figure 13). The site consists of a Pledger clay (very fine, smectitic, hyperthermic Typic Hapludert) with a shallow water table at 3- to 6-m deep. Transects were surveyed at two locations on this site with a Wenner electrode array. The first transect, measured 8 May 2013, spans 28 m at an electrode spacing of 0.5 m. The second transect, measured 9 May 2013, is shorter at 22.4

m due to a tighter electrode spacing of 0.4 m. Transect locations were selected based on accessibility for a truck with hydraulic soil coring device to pull soil samples from the heavily-forested site (Figure 14). Soil cores were collected 9 May 2013 to a maximum depth of approximately 4.5 m given an estimated depth-to-water table of 4 m (Miller and Bragg, 2007).


Figure 13: Dance Bayou Wildlife Area, part of the San Bernard National Wildlife Refuge (Satellite imagery from Google Earth).

Figure 14: Core truck positioned to pull samples at Dance Bayou site, 9 May 2013.

### 2.4. Resistivity Data Collection and Processing

Resistivity data were collected using the SuperSting according to the method described in Section 1.1. Surveys were named according to the date of collection in month-day-year format, so the BRS survey conducted 31 January 2013 was labeled 013113. Apparent resistivity data measured along each transect were transferred from the equipment to a desktop and inverted using EarthImager 2D (EI2D) inversion software (Advanced Geosciences, 2009). The inversion process interprets the volumetric averages of resistivity, measured as apparent resistivity, and attempts to assign resistivity values to specific locations throughout each transect. This process also attempts to reduce noise or error in the resulting model and acts according to user-set parameters

that govern the smoothness of the model. All apparent resistivity data sets were inverted using the same settings (see Appendix I) so each transect image can be compared. The inversion process concludes when an RMSE of less than 5% is achieved (Advanced Geosciences, 2009).

Resistivity values at locations matching the coring sites were extracted using the "Resistivity Logs" function of EI2D. The resistivity log for a given core consists of all resistivity values with pseudolocations falling the same horizontal distance from the survey origin as the collected core. Resistivity values were eventually compared to other characteristics of the soil at the same depth within the same core: volumetric water content and clay content.

### *Resistivity Images*

When raw resistivity data are imported into EI2D, the program automatically generates an apparent resistivity "pseudosection" – a map of apparent resistivity values at different depths and lateral positions (Everett, 2013a). A typical pseudosection produced in EI2D, such as the top image in Figure 15, is plotted with electrode number (beginning with 0) on the x-axis as a stand-in for distance. The true horizontal distance from the origin of the transect to the end is one less than the number of electrodes used, multiplied by the electrode spacing. Since all resistivity transects measured on the BRS in April 2013 used 56 electrodes at a spacing of 1 m, the electrode number is equivalent to the number of meters from the transect origin (Figure 15).

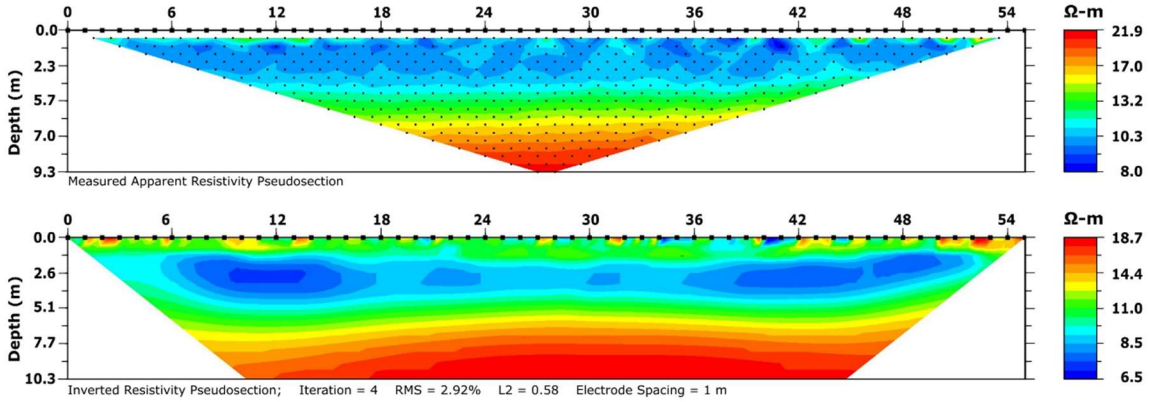


Figure 15: Measured apparent resistivity pseudosection (top) and inverted resistivity pseudosection (bottom) for Brazos River Site transect 040913, constructed using EarthImager 2D (Advanced Geosciences, 2009). Resistivity colors represent a log scale.

When the inversion process is complete, EI2D constructs an image like the bottom portion of Figure 15. The depth and resistivity scales do not typically match those of the apparent resistivity image, nor does the shape. While EI2D inverts and interpolates resistivity values spanning the entire plot area, the increasing distance of data under the beginning and end of the transect from the raw data points leads to poor resolution on the outer edges of the inverted image. The software automatically applies a "blanking feature" that hides these areas of the image — where inversion artifacts often occur — to prevent the viewer from drawing false conclusions from, or misinterpreting, the data. The blanking feature can be turned off, or the aspect ratio of horizontal offset-to-depth can be changed. An aspect ratio of 1.0 produces blanking at 45° from the depth axis. Increasing the ratio increases the degree of blanking. The degree of blanking may not be readily identified by visual inspection given the vertical exaggeration of the image (Advanced Geosciences, 2009).

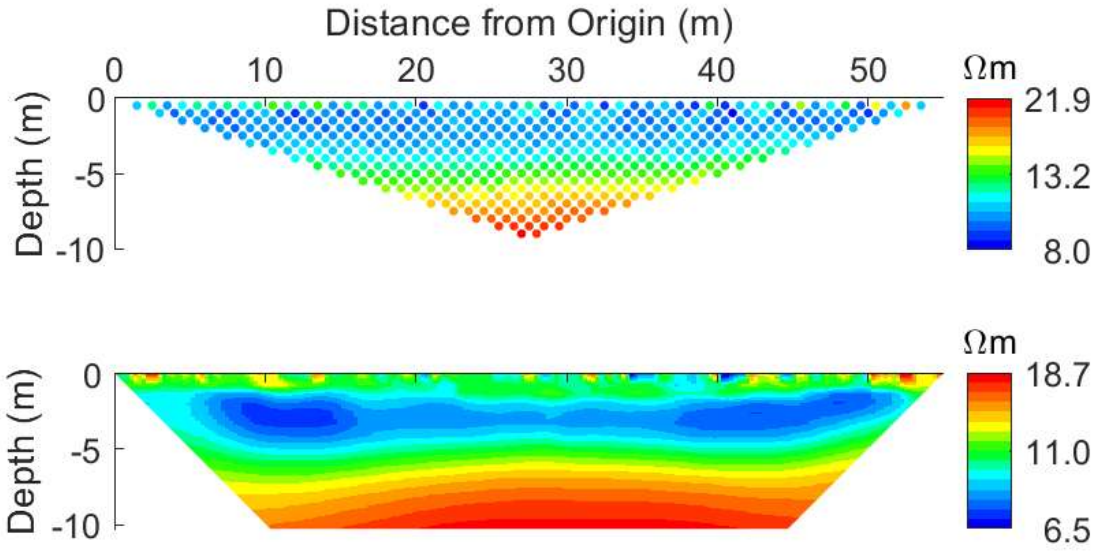


Figure 16: MATLAB-generated measured apparent resistivity pseudosection (top) and inverted resistivity pseudosection (bottom) for Brazos River Site transect 040913 using EarthImager 2D-style colormapping and data-driven colorscale.

Because the resistivity color scale is logarithmic and generated based on the maximum and minimum values of a given data set, among other issues, images from different surveys are often difficult to compare. To facilitate comparison across dates and sites, MATLAB code was written to produce images based on the requirements of the user, rather than the presets in EI2D. Figure 16 shows a MATLAB reproduction of the EI2D images for BRS transect 040913. Rather than representing raw resistivity data by plotting pseudolocations as black dots and applying an interpolated resistivity map behind the points (Figure 15, top), pseudolocations in the upper image were plotted as circles and filled with colors scaled to their respective apparent resistivity data. The EI2D colormap uses 16 color bins with pre-assigned RGB values and logarithmically scales the data to the colormap. To reproduce the colormap, RGB values were extracted

from the EI2D bins and logarithmically scaled to the raw data extracted from the SuperSting Output file.

The color scales of the EI2D images depended on the individual data sets; the MATLAB images, however, display all data sets with the same resistivity color scale for easy visual comparison. Furthermore, the non-monotonic variation of intensity of the color map used by EI2D may cause inappropriate interpretation of the data based on human perception, as well as introducing problems reproducing the figure in grayscale (Green, 2011; Rappaport, 2002). Accordingly, a cubehelix color map, developed by Green (2011), was chosen to make changes in resistivity easier to accurately distinguish by visual inspection. Figure 17 demonstrates the EI2D-style image with jet color map and data-dependent color scale, reproduced in MATLAB, compared to the cubehelix color image with standardized color scale corresponding to 0 to 25 ohm-m resistivity. Figure 17 shows the inverted resistivity data and pseudolocations output from EI2D inversion files at the top, while the bottom image shows the same data interpolated linearly on a 200x200 mesh with 45° blanking. Both images were produced in MATLAB.

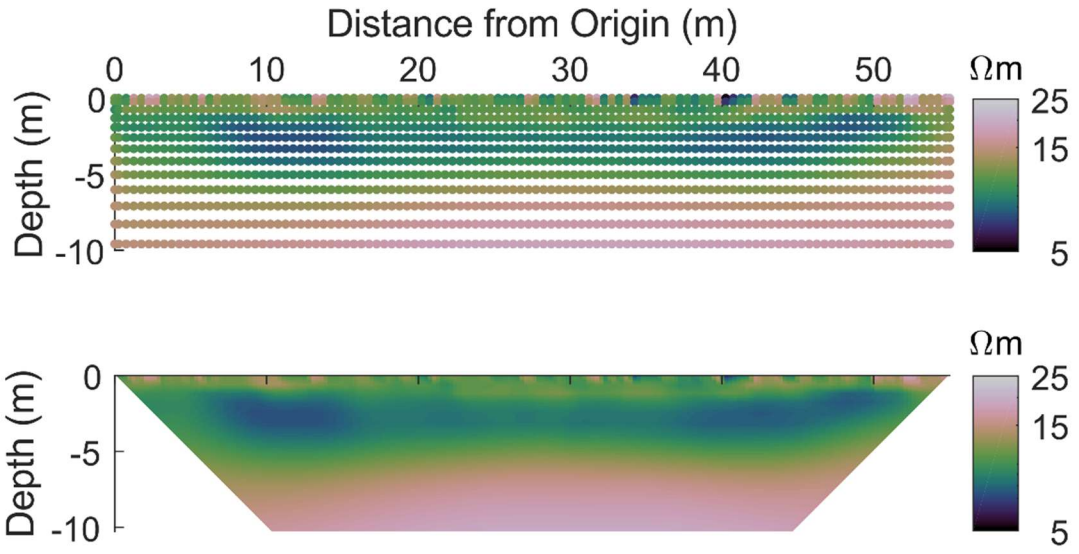


Figure 17: Inverted resistivity data plotted at corresponding pseudolocations (top) and interpolated pseudosection with 45° blanking (bottom) for Brazos River Site transect 040913. Cubehelix color map logarithmically-scaled to 5 to 25 ohm-m resistivity range.

### 2.5. Soil Core Collection and Processing

For the preliminary survey collected from the Brazos River Site in January 2013, two coring locations were selected based on estimates made from the inverted resistivity data: one with a region of suspected high soil moisture, the other with suspected low soil moisture. The first core was 5.49-m deep; the second was shallower at 3.80 m. Cores were divided into subsections of varying lengths, ranging from 0.10 to 0.65 m, based on natural breaks in the cores or observed changes in soil color, texture, or other features, as well as ease of sample transport. For all subsequent data collection at both sites, soil cores were pulled at three locations along each transect and were selected to capture the most variability observed in the ERT image while maintaining a distance of at least 3 m

between cores. For all core locations, the first several meters of coring depth were 0.06 m in diameter. Deeper cores had a diameter of 0.026 m. Using a narrower-diameter tube and pulling smaller soil volumes per sample reduced the load on the hydraulic soil coring machine and enabled greater coring depths. Core sections were divided into subsections of 0.05 to 0.30 m as they were pulled.

As cores were divided, individual subsections were placed into paper bags. Bagged samples were placed into gallon-sized plastic bags, which were sealed and placed in a large cooler. The cooler was kept in the shade to prevent evaporation in the samples and to facilitate transport of the samples from field to lab at the end of each sampling day.

Samples were weighed in their paper bags to determine the "wet weight" of each subsample in grams, then left on the lab countertop to air-dry. All DB samples, along with samples from four BRS cores, were dried to 60 °C and scanned with the Agri-Spec Vis/NIR unit for clay content prediction. Particle size distribution (Kilmer and Alexander, 1949) was measured on four or five samples per scanned core to compare against clay content predictions developed from reflectance spectroscopy. Samples that underwent laboratory particle size analysis were subsampled and weighed for soil moisture correction from air-dry to oven-dried weight.

All cores were subsequently dried to 105 °C and weighed, still in their original paper bags, to determine "dry weight" in grams. Soil volumetric water was calculated for each sample by subtracting dry weight ($W_D$) from wet weight ($W_W$) and dividing by the

volume of the subsection, which was calculated from the length ($l$) and diameter ($d$) of the subsection at time of coring (Equation 2).

$$\frac{W_W - W_D}{\pi \cdot l \cdot \left(\frac{d}{2}\right)^2} \qquad \textit{Equation 2}$$

Not all subsection lengths were well-defined enough to calculate soil volume and volumetric water content. Gravimetric water content was calculated for all subsections.

## 2.6. Data Analysis

*Data Preparation*

Analysis of the preliminary BRS survey from January 2013 consisted of plotting gravimetric water content data against depth for each core, and resistivity against gravimetric water content for both cores combined. Because length and diameter data had not been collected when the soil samples were pulled, an effort was made to predict volumetric water content from gravimetric. Volumetric water content data from other subsections at the BRS were plotted against their corresponding gravimetric data (Figure 18). The best-fit line (Equation 3), generated from over 900 data points, yielded an $r^2$ value of 0.87 and was used to predict volumetric data for the 013113 cores based on the 30 gravimetric data points available. The prediction was made according to

$$\theta = 1.79 \cdot w \qquad \textit{Equation 3}$$

where $\theta$ is volumetric water, $m^3\ m^{-3}$, and $w$ is the gravimetric water content in $kg\ kg^{-1}$.

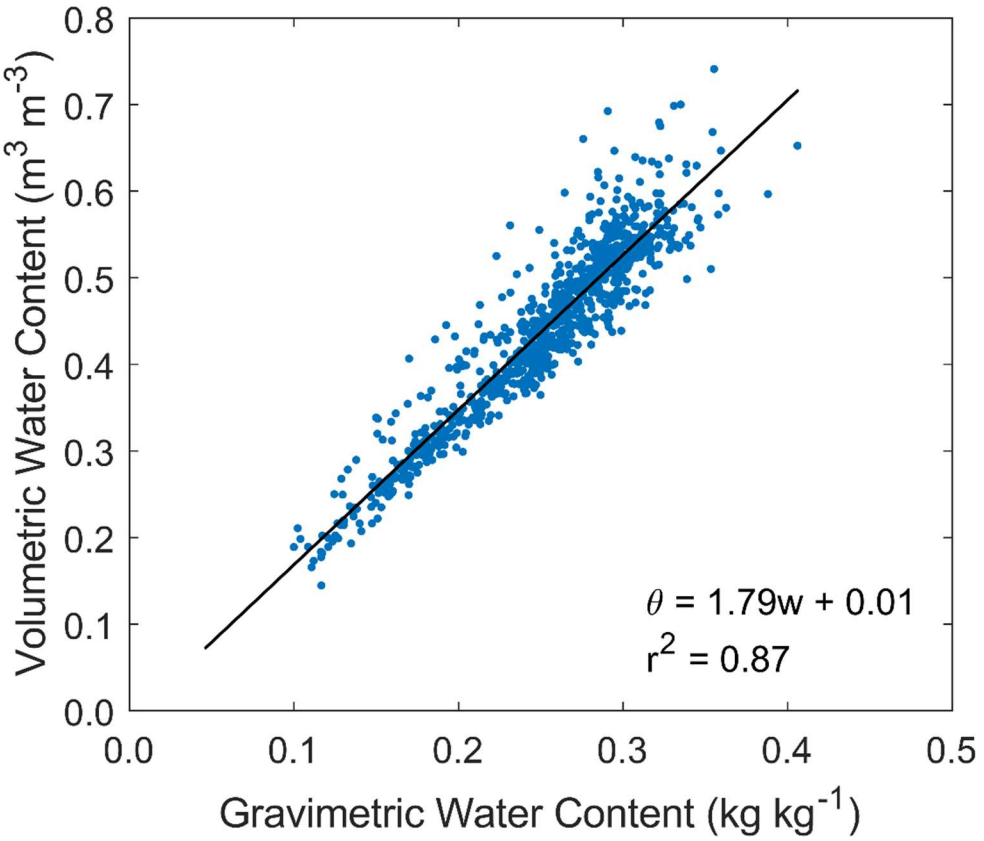


Figure 18: Volumetric ($m^3$ $m^{-3}$) vs. gravimetric (kg $kg^{-1}$) water content data and regression line for all April 2013 Brazos River Site data where both types were available.

Gravimetric water content data were also plotted with depth (Figure 19). An unexpected decrease in water content was observed between approximately 1.5 and 2.7 m depth. This range corresponds to an area of silt pockets noted while soil samples were collected from the field. Plotting inverted resistivity data against corresponding water content yielded an $r^2$ of 0.09 (Figure 20). Removing the data corresponding to silt pockets increased the coefficient of determination to 0.25 (Figure 21). The silt pockets

and their influence on the data led to the decision to estimate clay content where possible for future analysis.

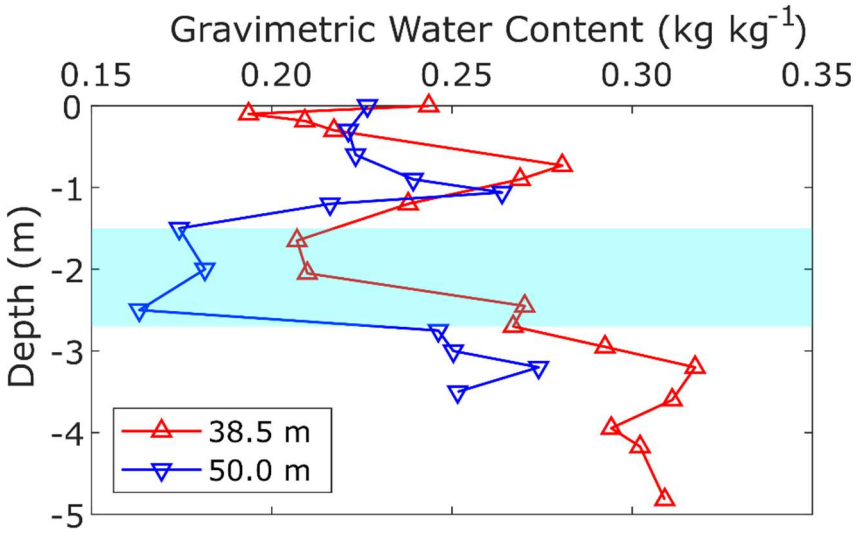


Figure 19: Brazos River Site transect 013113 gravimetric water content with depth.

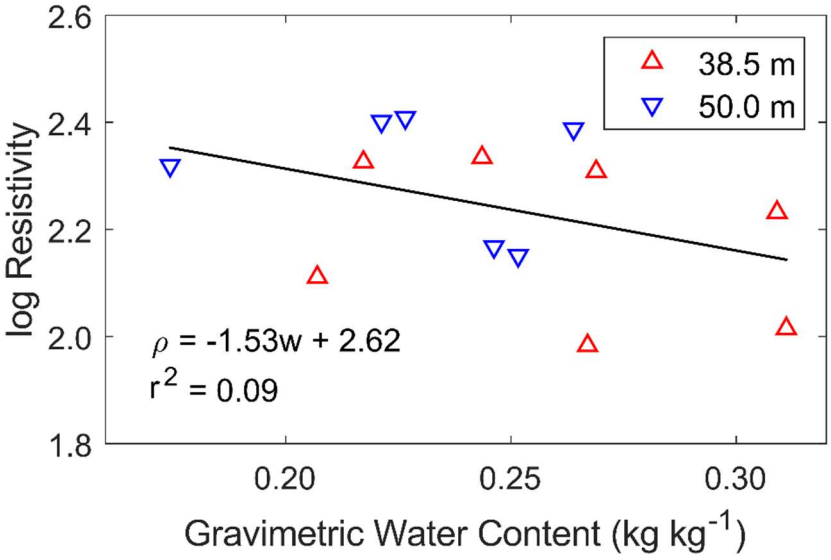


Figure 20: Brazos River Site transect 013113 log resistivity vs. gravimetric water content.

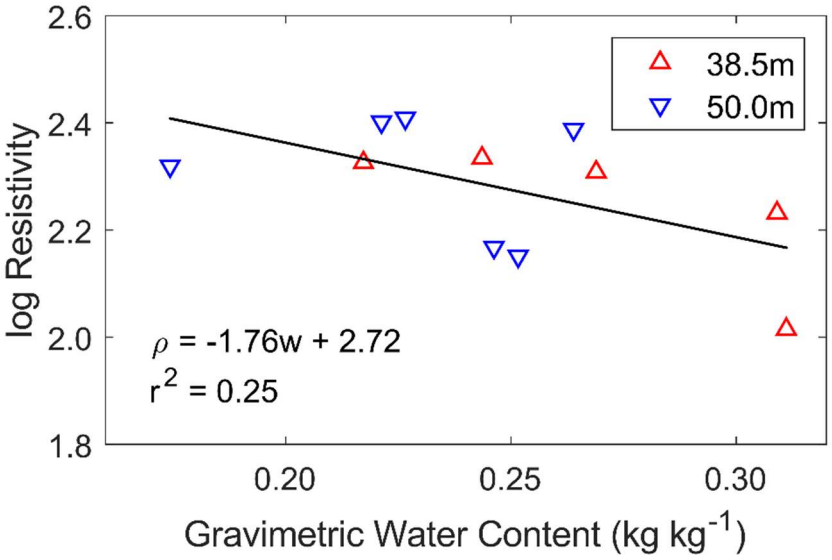


Figure 21: Brazos River Site transect 013113 log resistivity vs. gravimetric water content, suspected silt pockets removed.

Soil texture data were estimated with air-dry intact visible and near-infrared (Vis/NIR) scans of the soil cores. Scans were collected using a handheld probe with its own white light source. Scanning methods and equipment followed those of Waiser et al. (2007). The Vis/NIR spectra were converted to clay content using the Texas Soil Spectral Library models for air-dry in situ spectra (Ge et al., 2014). Waiser et al. (2007) noted a 6.1% RMSD and -2% bias for estimating clay content from dry intact soil cores. Furthermore, Vis/NIR is known to underpredict clay content in samples above 40%.

At the BRS, samples for PSA were selected based on inverted resistivity data extracted from transects 042513E and 042513W. Four samples were taken from each of the three cores in 042513W and from the northernmost core in 042513E (Table 2). The samples chosen corresponded to the highest and lowest resistivity values within the

depth of the core, as well as the two median values. Dance Bayou samples also were chosen based on resistivity but were taken from each of the six cores collected from the two transects (Table 3). DB cores had single median values and appear to have two minimum or maximum inverted resistivity values.

Table 2: Brazos River Site soil samples selected for PSA, identified by transect, core location in m from origin, and depth range in cm. Ranges corresponding to minimum inverted resistivity values are shaded in blue, median pair of values in green, and maximum values in orange.

| **Transect** | **042513W** | | | **042513E** |
|---|---|---|---|---|
| **Core** | 9.0 m | 34.0 m | 43.0 m | 9.0 m |
| **Depth range (cm)** | 185-193 | 60-75 | 0-15 | 0-15 |
| | 410-423 | 255-270 | 60-75 | 190-205 |
| | 490-505 | 330-345 | 245-260 | 405-420 |
| | 595-610 | 585-600 | 497-510 | 590-605 |

Table 3: Dance Bayou PSA samples identified by transect, core location in m from origin, and depth range in cm. Ranges corresponding to minimum inverted resistivity values are shaded in blue, median values in green, and maximum values in orange.

| **Transect** | **050813** | | | **050913** | | |
|---|---|---|---|---|---|---|
| **Core** | 7.5 m | 13.0 m | 20.0 m | 4.4 m | 14.4 m | 17.2 m |
| **Depth range (cm)** | 0-15 | 0-15 | 0-15 | 0-15 | 0-20 | 75-90 |
| | 60-75 | 30-45 | 30-45 | 95-110 | 65-80 | 155-170 |
| | 120-135 | 115-130 | 90-100 | 200-215 | 275-290 | 275-290 |
| | 345-355 | 345-360 | 355-370 | 230-245 | 320-334 | 320-335 |

*Temperature Correction*

Variations in soil temperature influence resistivity values for measurements collected in different weather conditions, different seasons, and different times of day (Rein et al., 2004). Ackerson et al. (2014), like Amidu and Dunbar (2007), applied a temperature correction to normalize the resistivity values collected throughout their research. Using an equation developed by Keller and Frischknecht (1966),

$$\rho_{25℃} = \rho_T[1 + 0.025(T - 25)], \qquad \textit{Equation 4}$$

where $\rho_T$ represents the bulk resistivity of the soil in ohm-m at temperature $T$ (°C), Ackerson et al. (2014) estimated the corresponding bulk resistivity had it been measured at 25°C, $\rho_{25℃}$ (ohm-m). Unlike Amidu and Dunbar (2007), their correction did not consider possible temperature variations with soil depth.

Rein et al. (2004) noted that, though temperature variations in the soil profile quickly diminish with depth, they "are significant in the upper part of the subsurface." While Michot et al. (2003) excavated a calibration pit layer by layer to install thermal probes and develop a temperature model, Amidu and Dunbar (2007) applied equations from Campbell and Norman (1998) to non-destructively estimate temperature variations with depth before applying the Keller and Frischknecht (1966) equation for bulk resistivity at 25 °C. Rather than disrupt the soil for in situ temperature measurements, the mathematical model was applied to BRS and DB data to estimate soil temperature before standardizing to 25 °C via Equation 4. Soil temperature, $T$ (°C), based on depth, $z$ (m), and local time of measurement, $t$ (hr), was estimated according to

$$T(z,t) = T_{ave} + A(0)\exp\left(-\frac{z}{D}\right)\sin\left[\omega(t - t_0) - \frac{z}{D}\right], \qquad \textit{Equation 5}$$

where $T_{ave}$ is the mean temperature (°C) for the day the ERT transect was measured, $A(0)$ is the amplitude of the changes in surface temperature on that date (°C), $D$ is the damping depth (m) and $\omega$ the angular frequency ($hr^{-1}$) for the diurnal cycle, and $t_0$ is a phase shift factor (Campbell and Norman, 1998). The time to measure each transect was at least an hour, so the time of measurement was selected to correspond with local weather station measurement times that fell between the start and end times of each transect measurement (Table 4).

Table 4: Summary of temperature data (°C) used in Equation 5 for each transect.

| Transect | $T_{ave}$ | $T_{max}$ | $T_{min}$ | Time measured | $t$ (hr) | Time of $T_{ave}$ | $t_0$ (hr) |
|---|---|---|---|---|---|---|---|
| **013113** | 10 | 19 | 1 | 11:53 AM | 11.88 | 9:53 AM | 10 |
| **040913** | 26 | 31 | 20 | 11:53 AM | 11.88 | 11:53 AM | 12 |
| **041113** | 13 | 20 | 6 | 8:53 AM | 8.88 | 12:53 PM | 12 |
| **041613** | 26 | 31 | 21 | 9:53 AM | 9.88 | 10:53 AM | 11 |
| **041913** | 13 | 19 | 6 | 8:53 AM | 8.88 | 10:53 AM | 11 |
| **042313** | 22 | 28 | 18 | 9:53 AM | 9.88 | 12:00 PM | 12 |
| **042513E** | 18 | 24 | 12 | 10:53 AM | 10.88 | 11:53 AM | 11 |
| **042513W** | 18 | 24 | 12 | 12:53 PM | 12.88 | 11:53 AM | 11 |
| **050813** | 20 | 27 | 14 | 3:53 PM | 15.88 | 7:53 AM | 8 |
| **050913** | 24 | 26 | 22 | 12:09 PM | 12.15 | 9:18 AM | 9 |

Equation 5 depends on two assumptions: 1) uniform soil properties throughout the depth considered, and 2) sinusoidally-varying temperature at the soil surface (Campbell and Norman, 1998). Silt lenses present in the soil profile of the BRS do interfere with this assumption, though they account for a relatively small portion of the data considered. While the temperature data for 042313 do approximate a sinusoidal pattern, a cold front moved in later in the day, skewing the average and mean temperatures. Accordingly, the time period considered when determining $T_{ave}$, $T_{max}$, and $T_{min}$ was shifted from 12:00 AM to 11:59 PM on 23 April 2013, to 12:00 PM on 22 April to 12:00 PM on 23 April. This made the average, maximum, and minimum temperature data more consistent with the conditions influencing the soil temperature at the time the transect was pulled.

The phase shift factor, $t_0$ (hr), for each transect was selected based on the time at which the air temperature first reached the average temperature for the date when the transect was measured. Because temperature data are discrete, making determination of the exact time when average temperature was reached impossible, the time when recorded temperature first reached or exceeded average temperature was rounded to the nearest hour to serve as the phase shift factor for that date (Table 4).

The amplitude, $A(0)$, is half of the peak-to-peak variation in soil surface temperature (°C), which is assumed to be sinusoidal on a diurnal, or daily, basis and can be calculated by subtracting the minimum temperature from the maximum temperature for the date of measurement and dividing by two. The damping depth is specific to the

type and properties of the soil medium: it is a function of the thermal diffusivity, κ ($mm^2$ $s^{-1}$), as well as the angular frequency of the sinusoidal variation in soil temperature in $s^{-1}$:

$$D = \sqrt{\frac{2\kappa}{\omega}} \qquad \textit{Equation 6}$$

Thermal diffusivity is the ratio of thermal conductivity to volumetric heat capacity. This value was estimated from Figure 22, adapted from Campbell and Norman (1998). The curve for clay soils is approximately linear and horizontal from 0.25 to 0.55 volume fraction of water, which corresponds with roughly 80% of the volumetric water content data collected between the two research sites. The thermal diffusivity value for this range of water content values appears to hover around 0.33 $mm^2$ $s^{-1}$ with minor fluctuations (Figure 22). Accordingly, this value was used to represent the thermal diffusivity of the soil in calculating damping depth via Equation 6.

In addition to thermal diffusivity, angular frequency, $\omega$, is needed to compute damping depth. Because changes in surface temperature are assumed to be sinusoidal in nature, both on a daily and annual basis, angular frequency represents how quickly the temperature fluctuates from one peak to the next. The equation

$$\omega = \frac{2\pi}{\tau} \qquad \textit{Equation 7}$$

can be used to calculate the annual angular frequency as well as the diurnal angular frequency. For the annual value, $\tau$ is equal to the number of seconds in one year, 31,536,000, and $\omega$ is $2 \times 10^{-7}$ rad $s^{-1}$. For both BRS and DB data, the interest is in the influence on resistivity data of temperature changes in the soil based on depth for the day

when the data were collected. For diurnal angular frequency, $\tau$ is the number of seconds in one day, 86,400, and $\omega$ is $7.3 \times 10^{-5}$ rad $s^{-1}$. With the diurnal angular frequency, $7.3 \times 10^{-5}$ rad $s^{-1}$, and estimated thermal diffusivity, 0.33 $mm^2$ $s^{-1}$, a damping depth of 95 mm was calculated according to Equation 6. For input into Equation 5, angular frequency was converted from $s^{-1}$ to $hr^{-1}$ and damping depth from mm to m. All data manipulation and preparation, including temperature correction, were conducted using MATLAB mathematical computing software (The MathWorks, Inc., 2018).

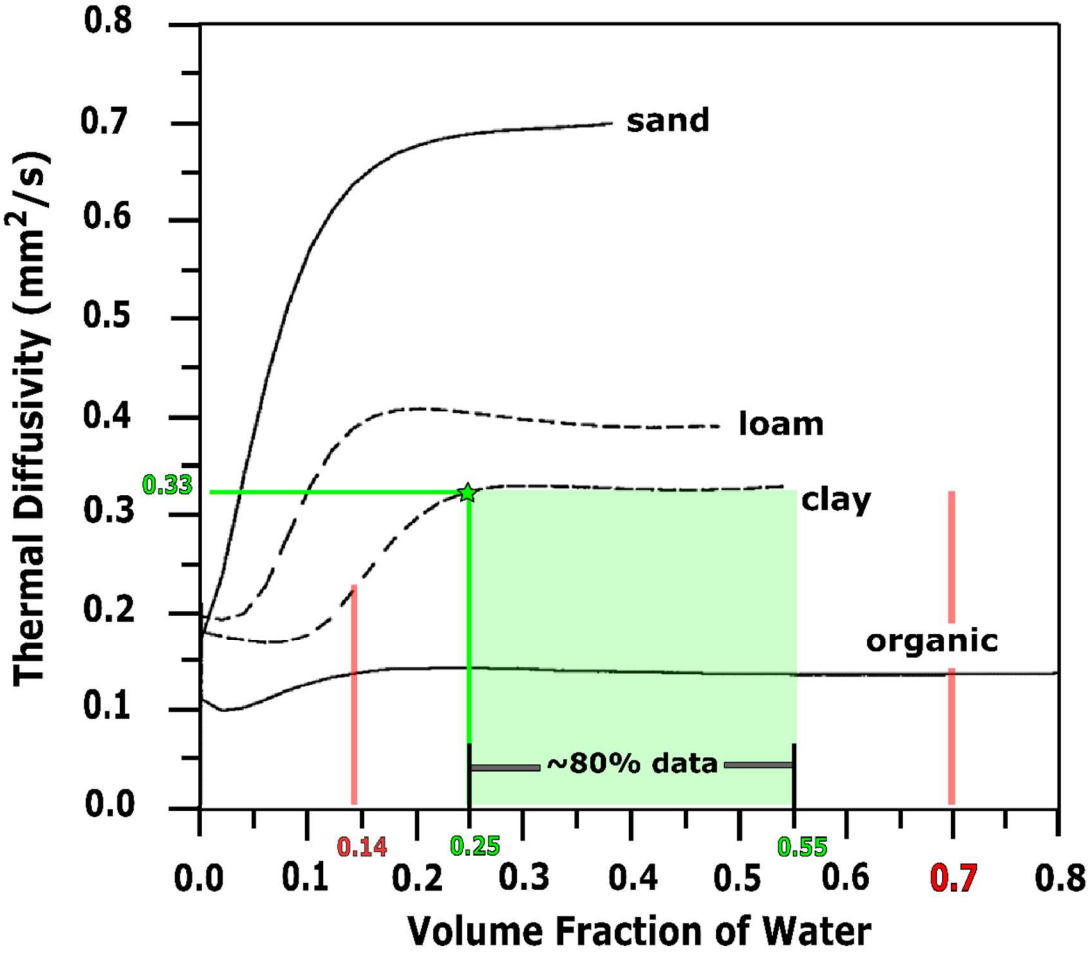


Figure 22: Thermal Diffusivity ($mm^2\ s^{-1}$) for various soil types plotted against volumetric water content ($m^3\ m^{-3}$). Maximum, minimum, and 80% range are shown for all volumetric water content data, as well as estimated thermal diffusivity used in temperature correction (Adapted from Campbell and Norman, 1998).

Historical weather data for all measurement dates were taken from Weather Underground (TWC Product and Technology, LLC, 2018), which provides daily maximum, minimum, and mean temperatures (Table 4), as well as hourly temperature readings, sourced from weather stations at airports nearest to each site. For the BRS, data were collected from Easterwood Airport's weather station, ID KCLL, near College

Station, Texas. The Dance Bayou sits roughly between Bay City and Angleton, Texas, and data from the two stations were consistently within 2 to 3 °C of each other on 8 and 9 May 2013. Ultimately, the weather station at the Brazoria County airport, ID KLBX, was chosen because the Dance Bayou lies in Brazoria County, and, based on aerial images of the station locations, the environment surrounding this airport appears most similar to that of the Dance Bayou.

### *Multiple Linear Regression*

Multiple Linear Regression (MLR) was conducted using R Statistical Software (R Core Team, 2017). Four models each were fit for two data set sizes: full data sets (Full) fit all available data, while three-variable data sets (Trim) considered only data points where log resistivity, clay content, and volumetric water content were all available. The models considered were log resistivity versus volumetric water content ($\mathrm{lnR} \sim \theta$), log resistivity versus clay content ($\mathrm{lnR} \sim \mathrm{C}$), volumetric water content versus clay content ($\theta \sim \mathrm{C}$), and volumetric water content versus clay content and log resistivity ($\theta \sim \mathrm{C} + \mathrm{lnR}$). Comparing $\mathrm{lnR} \sim \theta$ to $\theta \sim \mathrm{C}$ will establish whether log resistivity is a better predictor of water content than is clay content. The MLR model $\theta \sim \mathrm{C} + \mathrm{lnR}$ is most likely to be used in practical application of ERT data in Vertisols. Each of these models was applied to BRS data, DB data, and data from the two sites combined.

To determine whether MLR models for predicting water content based on clay content and log resistivity, the relationship of primary interest, are the same across multiple sites, analysis of covariance (ANCOVA) was conducted using a dummy variable to represent the two different study sites (Sheather, 2009). Data from both sites

for which log resistivity, clay content, and volumetric water content are available were used along with the dummy variable, "Site." For BRS data, "Site" was set to 0; DB data had "Site" set to 1. To test whether the slopes of the models were different between the two sites, an "unrelated regression lines" model was developed (Equation 8).

$$\theta = \beta_0 + \beta_1 \mathrm{C} + \beta_2 \ln\mathrm{R} + \beta_3 d + \beta_4 \mathrm{C} \times d + \beta_5 \ln\mathrm{R} \times d + e \qquad \textit{Equation 8}$$

In this equation, $\theta$ represents volumetric water content ($m^3\ m^{-3}$), C is percent clay content, lnR is log resistivity, $\beta_0$, $\beta_1$, $\beta_2$, and $\beta_3$ are regression coefficients, $d$ is the dummy variable, "Site", and $e$ is an error term. The regression coefficients $\beta_4$ and $\beta_5$ are measures of the changes in the magnitude of the effect that clay content and lnR have on $\theta$ based on the site where the data were collected. The significance of $\beta_4$ and $\beta_5$, established using Analysis of Variance (ANOVA), determines whether the slopes of the models for different sites are significantly different from each other.

If the slopes of the models are not determined to be significantly different, a "parallel regression lines" model is developed, where the dummy variable changes the predicted variable additively. If the MLR model comparing volumetric water content to log resistivity and clay content is represented by Equation 9, then the parallel regression lines model is represented by Equation 10, such as

$$\theta = \beta_0 + \beta_1 \mathrm{C} + \beta_2 \ln\mathrm{R} + e \text{ and} \qquad \textit{Equation 9}$$

$$\theta = \beta_0 + \beta_1 \mathrm{C} + \beta_2 \ln\mathrm{R} + \beta_3 d + e. \qquad \textit{Equation 10}$$

For DB, where $d = 1$, the term $\beta_3 d$ acts as an additional intercept, creating a regression line parallel to that of Equation 9. ANOVA is then used to determine whether the

intercepts of the MLR models are significant, which identifies whether “Site” is a significant predictor of volumetric water content. If “Site” is determined to be significant, then the MLR models are site-specific.

Models were also developed attempting to model change in water content over time based on corresponding changes in log resistivity. Cores pulled in April were divided into six groups within which comparisons were made. These groups were based on the distance of each core from the origin of its corresponding transect, so the cores in each group were within 3 m of the same distance from their respective origins (Figure 23). Trends in clay content data suggest that grouping the cores in this manner reduces possible variation in soil clay content from corresponding points within core groups. The smallest groups contain two cores and the largest contain four. Groupings selected are shown in Figure 23.

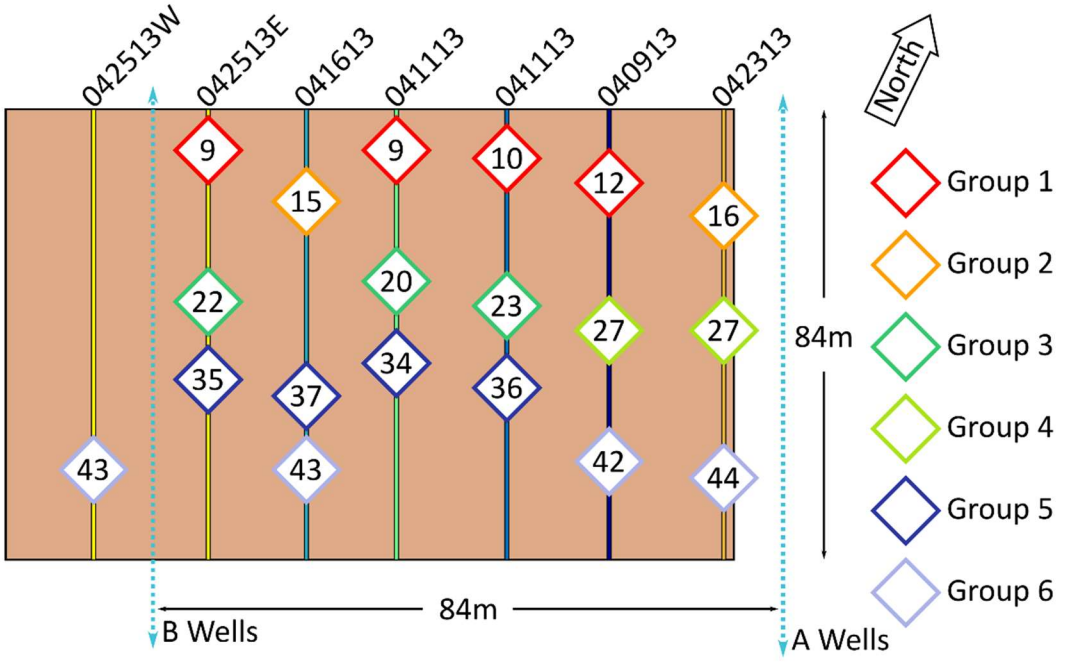


Figure 23: Approximate locations of Brazos River Site transects and cores assigned to groups for change over time analysis.

Because subsections of the various cores are not identical in length or position, depth bins were created that correspond to one resistivity data point whose pseudo-depth lies approximately at the center of the bin. Measurements of volumetric water content and, where possible, clay content from soil subsections whose depth ranges began inside a given bin were averaged into a single value per bin and data type. Bin-averaging data mimics the averaging effect inherent in ERT measurements and produces data values that correspond to consistent depths across different cores and transects. Seven bins (B) were used and labeled based on their depth order: B1 spans 0.0 to 0.5 m, B2 is 0.5 to 0.9 m, B3 is 0.9 to 1.5 m, B4 is 1.5 to 2.2 m, B5 is 2.2 to 3.0 m, B6 is 3.0 to 3.5 m, and B7 is 3.5 to 4.5 m. Though data are available for greater depths, the Ships clay layer is known

to be shallower further from the Brazos River. Using more bins spanning deeper within the profile would increase the likelihood of comparing data from the Ships clay to data from the underlying alluvium.

Resistivity data sets were inverted and treated individually, and differences in data between different pairs of transects were analyzed to simulate change over time. This method was described by Miller et al. (2008) and applied by Cardenas and Kanarek (2014). To construct data tables for linear regression, water content from a given group, bin, and transect was subtracted from water contents corresponding to the same group and depth on different transects, yielding $\Delta\theta$. The same was done with log resistivity values, resulting in ΔlnR. Data points from all transect pairs and bin depths were collected by group. Linear regression was conducted on all data for each group, followed by ANCOVA to determine whether the slopes of the models for different groups are significantly different from each other. If the model for any of the groups is significant, this would be evidence supporting the suitability of ERT for monitoring change in moisture over time in Vertisols.

# 3. RESULTS AND DISCUSSION

## 3.1. Soil Moisture Data

The range in volumetric water content data collected at both sites is 0.14 to 0.74 $m^3\ m^{-3}$ (Table 5). The range for the DB is smaller at 0.22 to 0.61 $m^3\ m^{-3}$. In a study conducted by Ackerson et al. (2014) on a Burleson clay Vertisol, a reduction in volumetric water content from 0.4 to 0.3 $m^3\ m^{-3}$ was noted to effect a change in resistivity of only 8% (Figure 24). For each of the transects considered in this study, 75% of the data are well above 0.3 $m^3\ m^{-3}$. This observation suggests that fluctuations in water content for most of the data should result in relatively small changes in resistivity for clay soils.

Table 5: Summary of volumetric water content data ($m^3\ m^{-3}$) for all Brazos River Site transects combined, all Dance Bayou transects combined, and all transects from both sites combined.

| Site | Min | Q1 | Median | Mean | Q3 | Max | Quantity |
|---|---|---|---|---|---|---|---|
| **Brazos** | 0.14 | 0.38 | 0.45 | 0.44 | 0.52 | 0.74 | 942 |
| **Dance Bayou** | 0.22 | 0.42 | 0.47 | 0.46 | 0.50 | 0.61 | 150 |
| **All Data** | 0.14 | 0.38 | 0.46 | 0.44 | 0.52 | 0.74 | 1,092 |

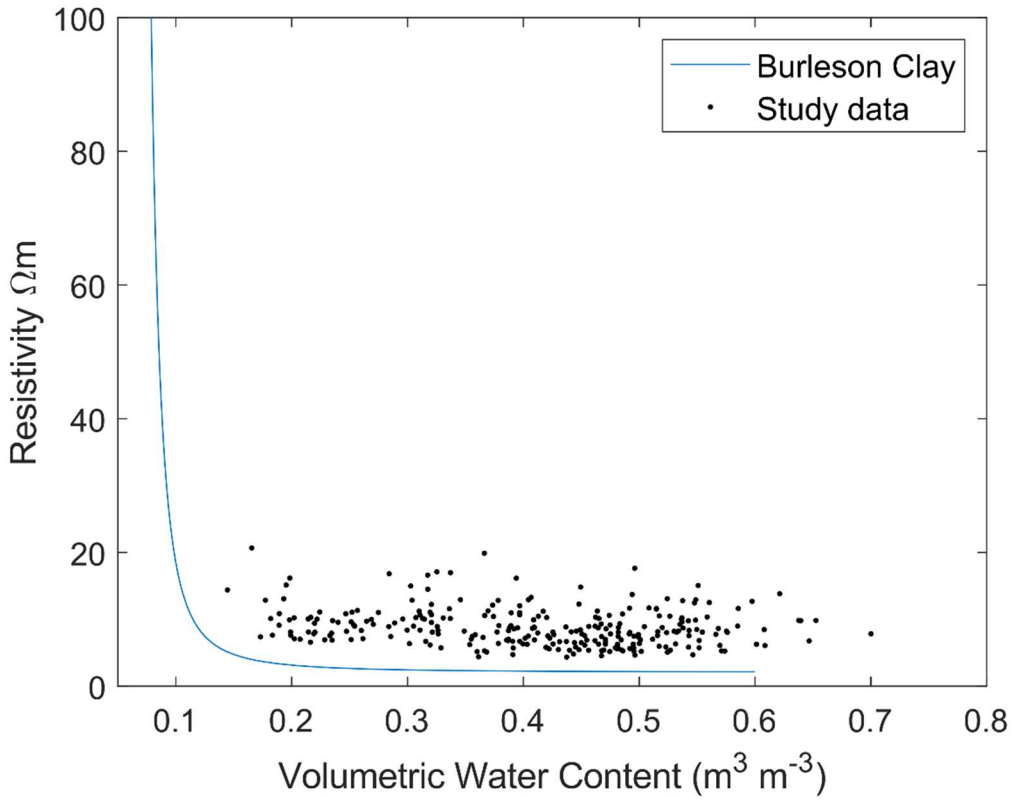


Figure 24: Brazos River Site and Dance Bayou data plotted over fitted curve for bulk soil resistivity (ohm-m) vs. volumetric water content ($m^3\ m^{-3}$) developed by Ackerson et al. (2014) for a Burleson clay Vertisol.

### 3.2. Soil Texture Data

Clay content from both the BRS and DB, along with visual observations made while collecting soil cores, show that the clay is not uniform throughout depth (Table 6). Clay content ranges from 22 to 76% at BRS, where 87% of the 376 data points exceed 40% clay content, falling into the clay texture classes. The range of the DB clay contents (n=155) is 14 to 75% with 90% of the data above 40% clay content. The average clay content for BRS and DB combined is 54%, with 88% of all data points equal to or greater than 40% clay content.

Table 6: Summary of percent clay content data for all Brazos River Site transects combined, all Dance Bayou transects combined, and all transects from both sites combined.

| Site | Min | Q1 | Median | Mean | Q3 | Max | Quantity |
|---|---|---|---|---|---|---|---|
| **Brazos** | 22.3 | 46.3 | 55.5 | 53.6 | 61.5 | 76.4 | 376 |
| **Dance Bayou** | 14.6 | 48.9 | 57.0 | 54.7 | 62.4 | 75.8 | 155 |
| **All Data** | 14.6 | 46.8 | 56.1 | 53.9 | 61.6 | 76.4 | 531 |

Particle size analysis for selected soil samples from both sites provides insight about percent sand and silt data in addition to percent clay. At BRS, PSA samples were selected from the two transects farthest from the Brazos River, where the clay layer should be shallowest and transition to sand occurs around 6 m (Munster et al., 1996). Of the 16 samples, 12 are classified as Clay, three as Clay Loam, and one as a Silt Loam (Table 7). Only six of the samples are composed of more than 2% sand. Of those six, the three samples with the lowest sand correspond to median resistivity values. The other three are each the deepest sample and correspond to the maximum resistivity values in their respective cores.

Particle size analysis results, visual analysis that occurred in the field as soil cores were pulled (Figure 25, top), and the well logs provided by Munster et al. (1996) suggest that sand is an inconsequential component of the soil profile until the bottom of the first layer of soil is reached. Reductions in clay content are countered by equal increases in silt content. Only after the bottom of the Ships clay layer (Figure 11) is reached does the sand fraction begin to increase substantially (Figure 25, bottom).

Table 7: Particle size analysis results from Brazos River Site samples. Ranges corresponding to minimum inverted resistivity values per core are shaded in blue, median pair of values in green, and maximum values in orange.

| Transect | Core | Depth | % Clay | % Sand | % Silt | Texture Class |
|---|---|---|---|---|---|---|
| 042513W | 9.0m | 185-193 | 36.3 | 0.8 | 62.9 | Silty Clay Loam |
| | | 410-423 | 68.2 | 0.2 | 31.6 | Clay |
| | | 490-505 | 61.9 | 7.0 | 31.1 | Clay |
| | | 595-610 | 50.8 | 17.8 | 31.4 | Clay |
| | 34.0m | 60-75 | 56.3 | 1.4 | 42.3 | Silty Clay |
| | | 255-270 | 68.1 | 0.2 | 31.7 | Clay |
| | | 330-345 | 58.2 | 0.3 | 41.5 | Silty Clay |
| | | 585-600 | 22.3 | 60.3 | 17.5 | Sandy Clay Loam |
| | 43.0m | 0-15 | 31.1 | 9.4 | 59.5 | Silty Clay Loam |
| | | 60-75 | 56.3 | 1.4 | 42.3 | Silty Clay |
| | | 245-260 | 68.6 | 0.0 | 31.4 | Clay |
| | | 497-510 | 68.0 | 1.2 | 30.8 | Clay |
| 042513E | 9.0m | 0-15 | 26.5 | 14.4 | 59.1 | Silt Loam |
| | | 190-205 | 42.5 | 0.4 | 57.1 | Silty Clay |
| | | 405-420 | 64.1 | 0.3 | 35.6 | Clay |
| | | 590-605 | 44.1 | 26.7 | 29.2 | Clay |

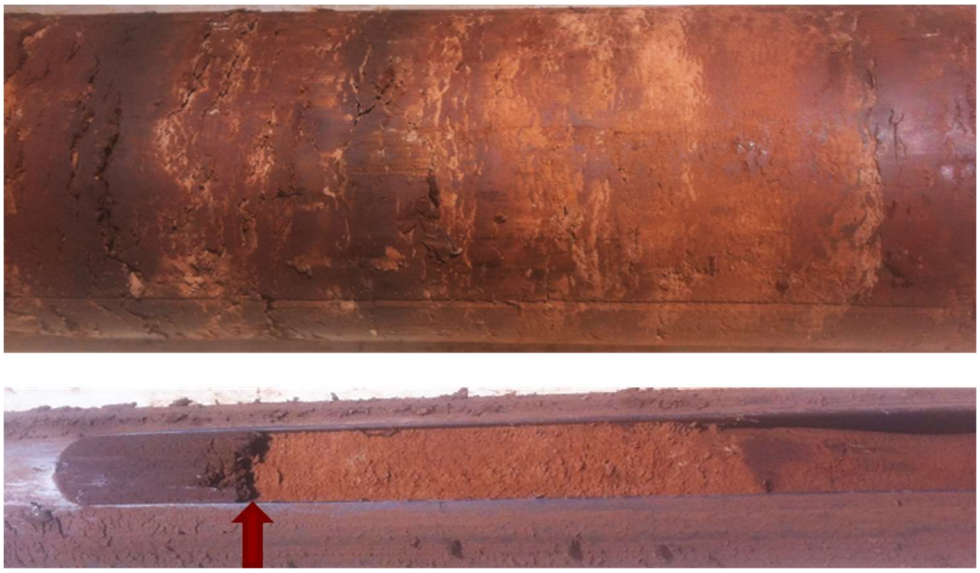

Figure 25: Subsections of Brazos River Site transect 042513W Core 34.0 m. Top shows variation in clay and silt content in upper depths. Bottom shows the transition between Ships Clay and unconsolidated alluvium layer, which is high in sand content. Red arrow marks transition point.

Table 8: Particle size analysis results from Dance Bayou samples. Ranges corresponding to minimum inverted resistivity values per core are shaded in blue, median pair of values in green, and maximum values in orange.

| Transect | Core | Depth | % Clay | % Sand | % Silt | Soil Type |
|---|---|---|---|---|---|---|
| 050813 | 7.5m | 0-15 | 67.51 | 2.90 | 29.59 | Clay |
| | | 60-75 | 65.29 | 4.60 | 30.11 | Clay |
| | | 120-135 | 57.37 | 4.70 | 37.93 | Clay |
| | | 345-355 | 14.63 | 69.10 | 16.27 | Sandy Loam |
| | 13m | 0-15 | 63.73 | 10.00 | 26.27 | Clay |
| | | 30-45 | 58.61 | 5.80 | 35.59 | Clay |
| | | 115-130 | 55.54 | 3.30 | 41.16 | Silty Clay |
| | | 345-360 | 71.89 | 0.20 | 27.91 | Clay |
| | 20m | 0-15 | 60.98 | 2.80 | 36.22 | Clay |
| | | 30-45 | 64.94 | 1.30 | 33.76 | Clay |
| | | 90-100 | 52.38 | 5.10 | 42.52 | Silty Clay |
| | | 355-370 | 66.24 | 0.20 | 33.56 | Clay |
| 050913 | 4.4m | 0-15 | 48.38 | 6.10 | 45.52 | Silty Clay |
| | | 95-110 | 43.54 | 10.20 | 46.26 | Silty Clay |
| | | 200-215 | 53.86 | 0.90 | 45.24 | Silty Clay |
| | | 230-245 | 54.46 | 0.30 | 45.24 | Silty Clay |
| | 14.4m | 0-20 | 34.58 | 26.30 | 39.12 | Clay Loam |
| | | 65-80 | 26.52 | 31.00 | 42.48 | Loam |
| | | 275-290 | 46.56 | 2.20 | 51.24 | Silty Clay |
| | | 320-334 | 56.00 | 0.40 | 43.60 | Silty Clay |
| | 17.2m | 75-90 | 27.98 | 27.80 | 44.22 | Clay Loam |
| | | 155-170 | 40.62 | 11.10 | 48.28 | Silty Clay |
| | | 275-290 | 56.36 | 0.50 | 43.14 | Silty Clay |
| | | 320-335 | 46.55 | 0.60 | 52.85 | Silty Clay |

At the DB, PSA was conducted on four samples from each of the six cores collected. Of the 24 samples analyzed, 20 are classified as Clay or Silty Clay (Table 8). Two samples are Clay Loam and the other two are a Sandy Loam and a Loam. The DB samples generally have more sand than the BRS soils. The three samples with the largest sand fraction correspond to maximum resistivity values for their respective cores.

Figure 26: Subsections of Dance Bayou cores pulled 9 May 2013. Top shows blackish soil similar to that found in bowl formations by Miller and Bragg (2007), while bottom shows lighter brown soil with red and darker brown mixed in.

Visual observations as DB cores were pulled included drastic color changes from near black to light brown, pockets of reddish clay, and even areas of noticeable concentrations of carbonates (Figure 26). Blackish soil likely comes from higher amounts of soil organic carbon often found in bowl formations common to Vertisols

(Figure 3). Reddish and brown clay are characteristic of the parent material of the Bottomland Hardwood Vertisols, with the Permian Red Beds thought to be the source of the reddish ferric-oxide pigment (Miller and Bragg, 2007).

### 3.3. Resistivity Data and Images

Multiple linear regression models were applied to the three data treatments – INV, T25, and TC_25 – to determine which treatment produced the best models. The four models listed in Section 2.4 were conducted for both Full and Trim sets, as well as for BRS, DB, and Combined data – 24 models in all. For ten of the models, the adjusted $r^2$ values were nearly identical across the three data treatments. In most of the other 14 models, the TC_25 models had adjusted $r^2$ values as high as or higher than the INV models. For twelve of the models, T25 had the lowest $r^2$ values of the three treatments. Subsequent data analysis focuses only on TC_25 data.

Table 9 summarizes the treated resistivity data for all BRS transects, all DB transects, and all transects combined. While BRS produced the overall minimum resistivity value, DB data are generally lower than BRS data. The mean BRS value, 9.01, is 0.6 ohm-m higher than the DB mean; the value denoting the third quartile for BRS is nearly 1.6 ohm-m higher than the DB value, 8.88, and the maximum BRS value is nearly 3.5 ohm-m higher than the DB maximum of 17.10 ohm-m.

Table 9: Summary of Resistivity data in ohm-m for individual transects from both sites, all Brazos River Site transects combined, all Dance Bayou transects combined, and all transects combined.

| Transect/**Site** | **Min** | **Q1** | **Median** | **Mean** | **Q3** | **Max** | **Quantity** |
|---|---|---|---|---|---|---|---|
| 013113 | 4.54 | 5.32 | 6.29 | 6.20 | 6.83 | 8.72 | 12 |
| 040913 | 7.41 | 8.61 | 9.70 | 9.92 | 11.06 | 13.70 | 28 |
| 041113 | 4.80 | 6.41 | 7.16 | 7.37 | 8.12 | 12.02 | 27 |
| 041613 | 8.75 | 9.96 | 10.46 | 11.09 | 11.60 | 17.64 | 28 |
| 041913 | 5.27 | 6.85 | 7.81 | 8.06 | 9.46 | 11.62 | 28 |
| 042313 | 4.64 | 6.18 | 8.63 | 8.57 | 10.72 | 14.39 | 28 |
| 042513E | 5.56 | 7.75 | 9.92 | 10.09 | 12.27 | 20.67 | 29 |
| 042513W | 4.34 | 6.76 | 8.93 | 9.14 | 10.56 | 19.88 | 29 |
| **Brazos** | 4.34 | 7.00 | 8.74 | 9.01 | 10.47 | 20.67 | 217 |
| 050813 | 5.24 | 5.71 | 6.27 | 6.46 | 7.46 | 8.46 | 29 |
| 050913 | 6.63 | 8.01 | 8.60 | 9.96 | 11.80 | 17.10 | 37 |
| **Dance Bayou** | 5.24 | 6.31 | 7.93 | 8.41 | 8.88 | 17.10 | 68 |
| **Combined** | 4.34 | 6.83 | 8.32 | 8.87 | 10.27 | 20.67 | 285 |

*Brazos River Site*

Figure 27a shows the preliminary BRS measurement conducted 31 January 2013. Over the course of the month of January, a nearby weather station measured a total of 129 mm (5.06 in) of precipitation and an average of the mean daily temperatures for the month of 12 °C (54 °F). Under these weather conditions, it is likely that the soil profile was relatively wet, though the range and average of the water content data available for this transect are not noticeably different from those of other transects. A wetter profile would theoretically produce the large areas of dark blue visible in the image. This

transect was also the closest to the Brazos River, where the clay layer is deepest. The combination of the deeper clay layer and likely wet profile may explain why this transect image shows a consistent and relatively low resistivity throughout most of the profile.

By 9 April, when BRS transect 040913 was pulled, 23 mm (0.89 in) of precipitation had occurred, mostly in the first few days of the month. Temperatures in the days leading up to measurement averaged around 70 °F and reached as high as 87 °F day-of. The soil was likely drier than that of the 013113 transect, resulting in the lower resistivity values seen in Figure 27b. The transect is also farther from the Brazos River, so the depth of the clay layer is shallower, though no clay content data are available for this transect. As soil cores were pulled, dark clay was noted beginning around 5.5 m deep in Cores 1 and 3. Sand was not visible in any of the cores, despite reaching a depth of 6 m in two of the cores.

The upper 5 m of BRS transect 041113 (Figure 27c) would typically be interpreted as being wetter than the corresponding region of BRS 040913 given the generally lower resistivity mapped in that area. Though a light precipitation event of 4.32 mm (0.17 in) occurred on 10 April, the summary statistics for volumetric water content on 9 April and 11 April are similar with means of 0.47 and 0.45 $m^3\ m^{-3}$, respectively, and maxima of 0.74 and 0.70 $m^3\ m^{-3}$, respectively. This transect is the first in time for which clay content are available. The first core, which is 10 m from the transect origin, ranges in clay content from 23 to 68% with a mean of 52%. Knowing that sand within the Ships clay is generally no more than 2%, the soil type for this region is predominantly clay or silty clay with a few pockets of silty clay loam.

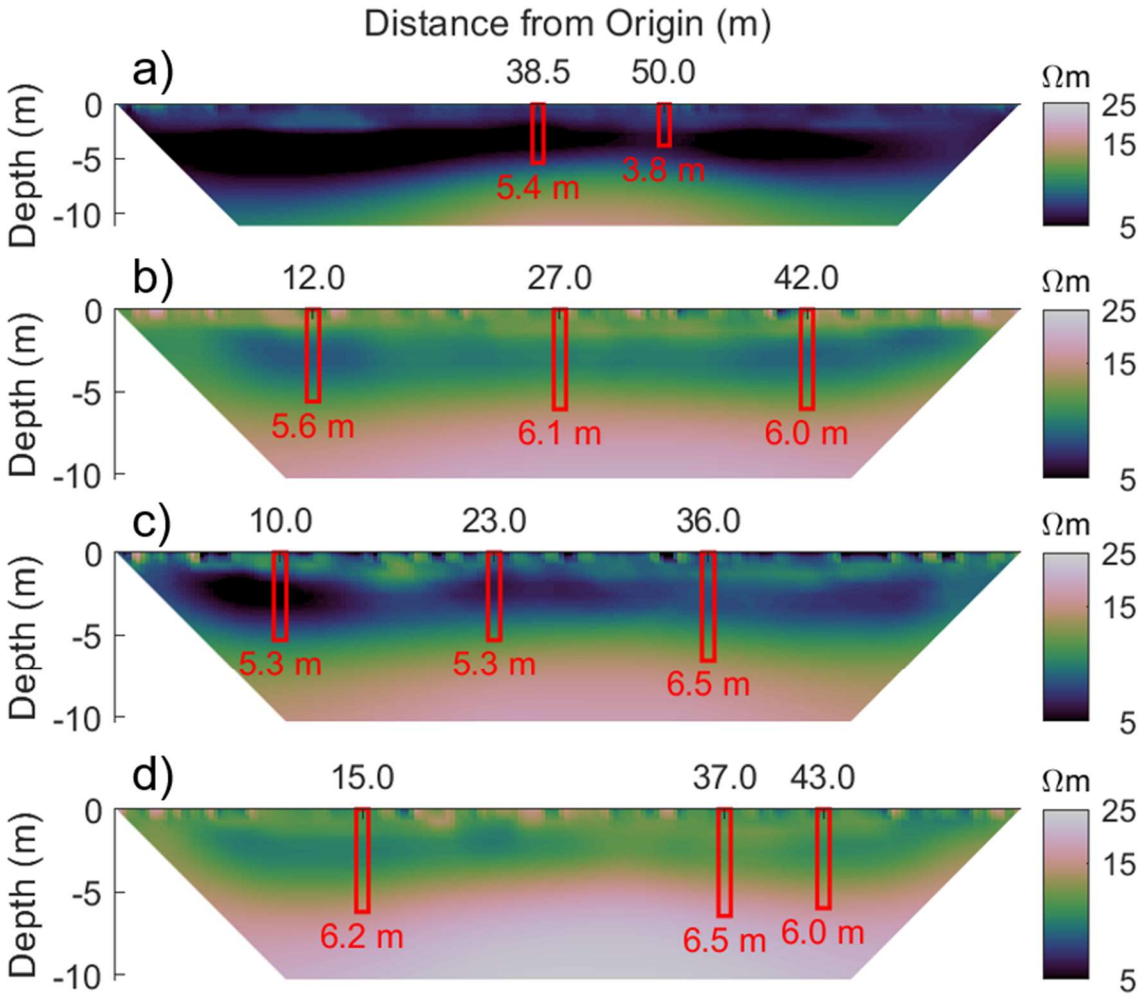


Figure 27: Brazos River Site transects: a) 013113 – 112-m long b) 040913, c) 041113, and d) 041613 all 56-m long; cores labeled in red:.

Neither the first nor second core reaches into the sand layer, though sand was observed in the third core, 36 m from the origin, around 6.2-m deep. Figure 27c shows the resistivity in the bottom of the third core rising toward 15 ohm-m. The volumetric water content begins to drop below 0.4 $m^3$ $m^{-3}$ around 6-m deep and reaches 0.21 $m^3$ $m^{-3}$ at the bottom of the core. Increasing resistivity in this region could be a result of changing soil texture, decreasing water content, or both.

No precipitation was registered between 9 and 16 April 2013. The upper 5 m region of Figure 27d displays resistivity values that are generally higher than corresponding regions of other BRS transects. Volumetric water content is 0.20 to 0.52 $m^3$ $m^{-3}$ in this area of transect 041613, which matches closely with the range of the bottom 75% of water content data for this transect: 0.18 to 0.52 $m^3$ $m^{-3}$. Clay content data are only available for the upper 2.3 m of the first core and range from 42 to 70%. Black soil appeared beginning around 5.5-m deep in cores one and two, and sand was logged at 6-m deep in core three.

Between 16 and 19 April, 8.64 mm (0.34 in) of rain fell, likely accounting for much of the increase in resistivity evident between Figure 27d and Figure 28a. Once again, the summary statistics for volumetric water content do not show much change between the two dates or would suggest that the three cores pulled on 19 April are slightly drier than the three pulled on 16 April. Clay content data are available for the upper 2.5 to 3.0 m of the first and third core and all of the second core. While pockets of silty clay loam are visible in Cores 9.0 m and 34.0 m, Core 20.0 m is at least 40% clay throughout its depth and is silty clay or clay for all samples. Mean and maximum clay content are 58% and 69%, respectively. As cores were pulled, sand was noted at the bottom of the first core around 6.25-m deep. Black soil was noted beginning near 5.5-m deep in the second and third cores. It is unclear whether the change in soil color corresponds to change in soil texture or influences resistivity.

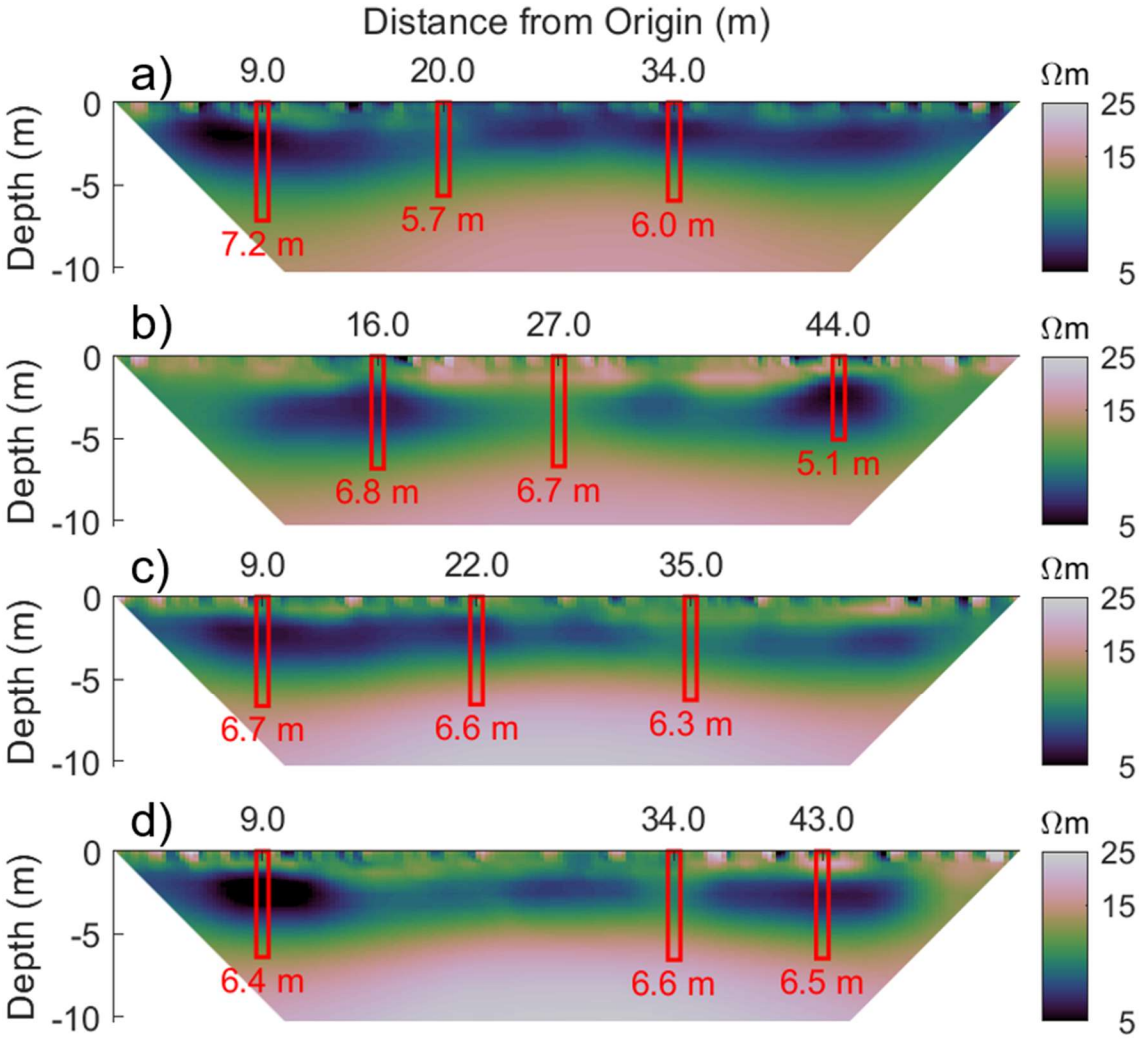


Figure 28: Brazos River Site transects: a) 041913, b) 042313, c) 042513E, d) 042513W; cores labeled in red. All transects 56-m long.

Figure 28b shows unusual variability in resistivity within the upper 5 m region of the image compared to other BRS transect images. No precipitation occurred between 19 and 23 April, so low resistivity levels in the upper 1 to 2 m of soil likely result from evapotranspiration as temperatures continue to rise. Surficial cracking as the clay began to shrink may also have caused high resistivity values visible near 20, 30, 40, and 50 m

from the transect origin. The minimum water content for the entire study, 0.14 $m^3$ $m^{-3}$, was observed in this transect, along with a mean value of 0.44 and maximum of 0.60 $m^3$ $m^{-3}$. Clay content was available for only one core but reached 6.7-m deep without dropping below 40%. Sand was visible at the bottom of this core starting around 6.5 m, which corresponds with both the minimum water content and a high clay content value of nearly 58%.

Transects 042513E and 042513W, measured on the same day, are the two transects furthest from the river: 042513E (Figure 28c) is on the eastern side of the 'B' well nests (Figure 10), while 042513W (Figure 28d) is to the west. Well nest logs record the clay layer extending to 6 m at the southernmost wells and 7 m to the north (Table 1).

As 042513E cores were pulled, sand was noted beginning around 6 m in Cores 2 and 3 to the south, and 6.25 m in Core 1 toward the north. Slightly higher resistivity values at the bottom of Core 1 compared to the other two cores seem to agree with this pattern. Core 1 is this first BRS core for which PSA results are available, showing that sand content jumps from 0.3% in the 4.05 to 4.2 m depth range to 26.7% percent for 5.90 to 6.05 m, where the soil is still classified as a clay. Clay content is available for all of Core 1, ranging from 26 to 76%, and the upper 2.5 m of Core 2, ranging from 26 to 68%. All summary statistics from Core 2 are lower than for Core 1, suggesting that higher clay contents are reached deeper in the Ships clay than clay data for Core 2 are available. While Figure 28c seems to suggest that Core 3 is the driest, Core 2 has lower summary statistics. Core 1 has the highest summary statistics for both moisture and clay content. Volumetric water content in the region of Core 2 for which clay content is

available ranges from 0.17 to 0.46 $m^3$ $m^{-3}$. This corresponds closely to the lower 50% of water content data for Core 1: 0.20 to 0.46 $m^3$ $m^{-3}$. For all Core 2 data, the lower 50% of water content data is 0.17 to 0.45 $m^3$ $m^{-3}$ with average and maximum values of 0.43 and 0.58 $m^3$ $m^{-3}$, respectively. Despite the low resistivity values in the upper portion of Core 2, volumetric water content is also low in this region.

Transect 042513W (Figure 28d) is the only BRS transect for which clay content is available for all soil samples (Figure 29). Sand became visible in Core 2 between 5.70 and 5.85 m deep, and PSA results for the sample immediately following classify the soil as Sandy Clay Loam from 5.85 to 6.00 m. In Core 3, black soil was noted from 5.10 to 5.95 m with clay content ranging from 43 to 62%. The black soil quickly transitioned to fine sand around 5.95 m. Resistivity values at the bottom of Cores 2 and 3 seem to match up with the changing soil composition. Though sand was not noted at the bottom of Core 1, PSA results show an increase in sand beginning around 5.0 m at 7% and reaching 17.8% sand near 6.0 m. Core 2 PSA results show sand content reaching 60.3% around 6.0 m. The Ships clay layer is known to increase in depth moving northward, so it is unsurprising that the northernmost core (Core 1) transitions to sand at a greater depth than cores farther south. Overall, clay content ranges from 22 to 75%, with Core 3 having the highest summary statistics of the individual cores for this transect. Water content for the transect ranges from 0.17 to 0.65 $m^3$ $m^{-3}$. Core 2 generally has lower summary statistics for water content than the other cores, which agrees with the transect image. Cores 1 and 3 pass through regions of dark blue, the lowest resistivity values,

while Core 2 is mainly green before transitioning to higher resistivity levels nearing the bottom of the Ships clay (Figure 28d).

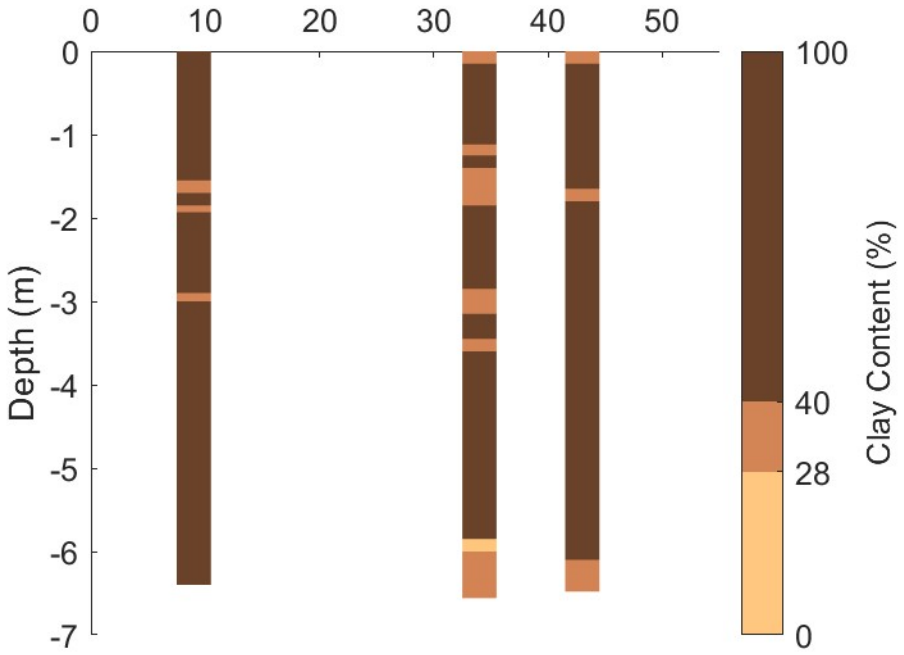


Figure 29: Brazos River Site transect 042513W, percent clay content with depth for all three cores: 9 m, 34 m, and 43 m from the origin.

*Dance Bayou*

The first DB transect is more uniform in resistivity than the second transect (Figure 30a). In the first core, 75% of the data are above 54% clay content, with only three core subsections having less than 49% clay. These three soil sections constitute the bottom 0.40 m of the core and have clay contents of 15, 28, and 34%. While resistivity and volumetric water content data are not available for the bottom two subsection depths, the sample with 15% clay, which begins at 3.45 m depth, has the highest

resistivity at 9.22 ohm-m and lowest water content at 0.45 $m^3$ $m^{-3}$. In Cores 2 and 3, all the data are above 51% and 48% clay content, respectively, and 0.45 and 0.39 $m^3$ $m^{-3}$ in water content, respectively. Trace amounts of sand ranging from 0.2 to 10% were measured and observed to increase with depth.

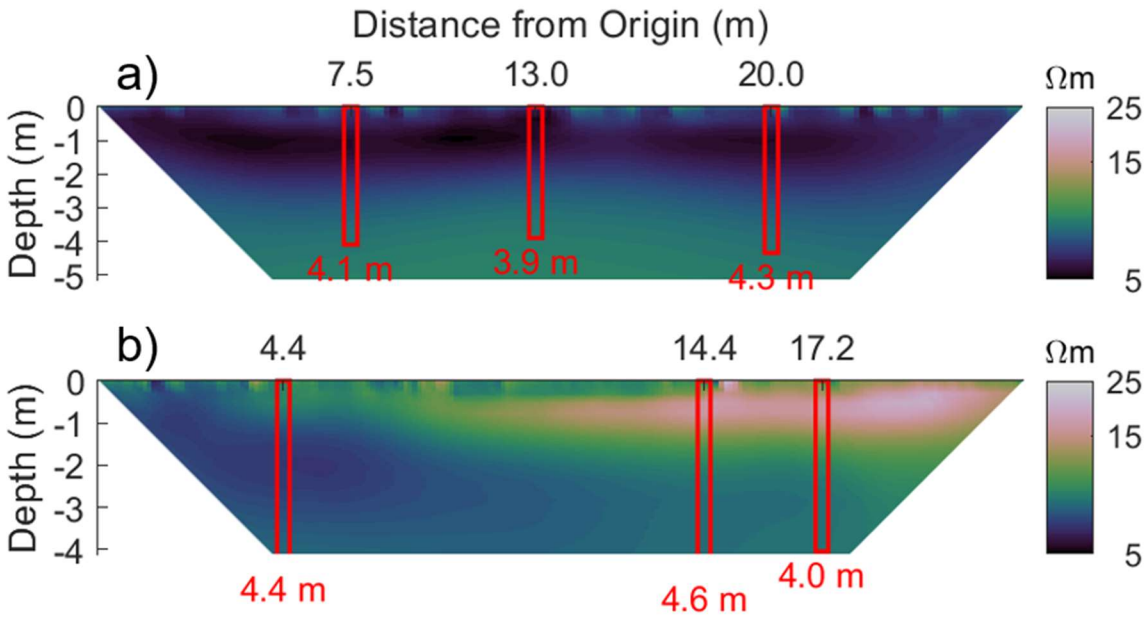


Figure 30: Dance Bayou transects: a) 050813, 28 m long, and b) 050913, 22 m long; cores and corresponding depths labeled in red.

Though transect 050813 shows increasing resistivity values with depth (Figure 30), only the data in the first core display changes in water content and clay content that should correspond to increasing resistivity. It is possible that similar changes take place deeper into the soil profile than the other two cores reached; the averaging nature of ERT and inversion methods could have resulted in a smoother decrease in resistivity values

rather than an abrupt change where physical changes in the soil are occurring. Variations in the color of the soil (Figure 26), noted as cores were pulled, indicate bowl and chimney features also noted by Miller and Bragg (2007).

Transect 050913 (Figure 30b) is markedly different from 050813. Core 1, in the westernmost region of the transect, is the most similar to transect 050813 of the three 050913 cores. All three cores from transect 050813 have resistivity ranges from approximately 6.0 to 9.5 ohm-m. Core 1 from transect 050913 ranges from 6.8 to 9.2 ohm-m. The other two cores have resistivity ranges from approximately 8.2 to 17.5 ohm-m, a difference that can be clearly seen in Figure 30b. Summary statistics for clay content data in Core 1 are generally similar to the three 050813 cores, though the minimum and first quartile values are lower. Clay content generally increases with depth for Core 1, though no other pattern is readily distinguishable from the data. The lowest clay content, 34%, occurs near a depth of 3 m, as was seen in the three 050813 cores. For 050913 Cores 2 and 3, the lowest clay contents fall within the first two meters of soil with a range of 21 to 52% clay between the two cores. Below two meters, clay content ranges from 43 to 76%. This trend is reflected by the distinct color changes in Figure 30b. For each of the three cores, the lowest water content values occurred in the first 2.5 m of soil. Below 2.5 m, water contents cluster between 0.45 and 0.60 $m^3$ $m^{-3}$. This trend is likewise reflected in the resistivity image for this transect.

Sand content increases from Core 1 to Core 2, while the sand content for Core 3 is similar to that of Core 2. Core 1 varies between 6 and 10% sand in the samples with

PSA data, while Cores 2 and 3 vary from 26 to 30% sand. Resistivity values appear to vary directly with sand content (Figure 30b).

### 3.4. Regression Analysis

*Brazos River Site*

At the Brazos River Site, linear regressions of log resistivity and volumetric water content yielded highly-varied results in terms of slope sign and $r^2$ values.

Table 10: Summary of log resistivity vs. volumetric water content linear regression models for individual and combined Brazos River Site transects.

| Transect | Slope | p-value | $r^2$ | DOF |
|---|---|---|---|---|
| **013113** | -1.02 | 0.23 | 0.13 | 11 |
| **040913** | -0.13 | 0.67 | 0.01 | 26 |
| **041113** | 0.13 | 0.69 | 0.01 | 26 |
| **041613** | 0.75 | 0.004 | 0.28 | 26 |
| **041913** | 0.07 | 0.85 | 0.00 | 26 |
| **042313** | -1.40 | 0.003 | 0.29 | 26 |
| **042513E** | -0.67 | 0.13 | 0.09 | 26 |
| **042513W** | -0.23 | 0.64 | 0.00 | 27 |
| **Combined** | -0.29 | 0.09 | 0.01 | 208 |

Two of the transect models summarized in Table 10 show slope values significantly different from zero (p-value <0.05), though one slope is positive (Figure 31a) and the other is negative (Figure 31b). If resistivity is responding to soil water content directly, the slope is expected to be negative. The $r^2$ values for these two models are the highest

from Table 10 at 0.28 for 041613 and 0.29 for 042313. Combining data for all BRS transects yields a regression model with a negative slope, significant for alpha value 0.1, but with an $r^2$ value of only 0.01 (Figure 32). The regression models for log resistivity and volumetric water content using BRS data suggest that, for this site, log resistivity alone is not useful for measuring volumetric water.

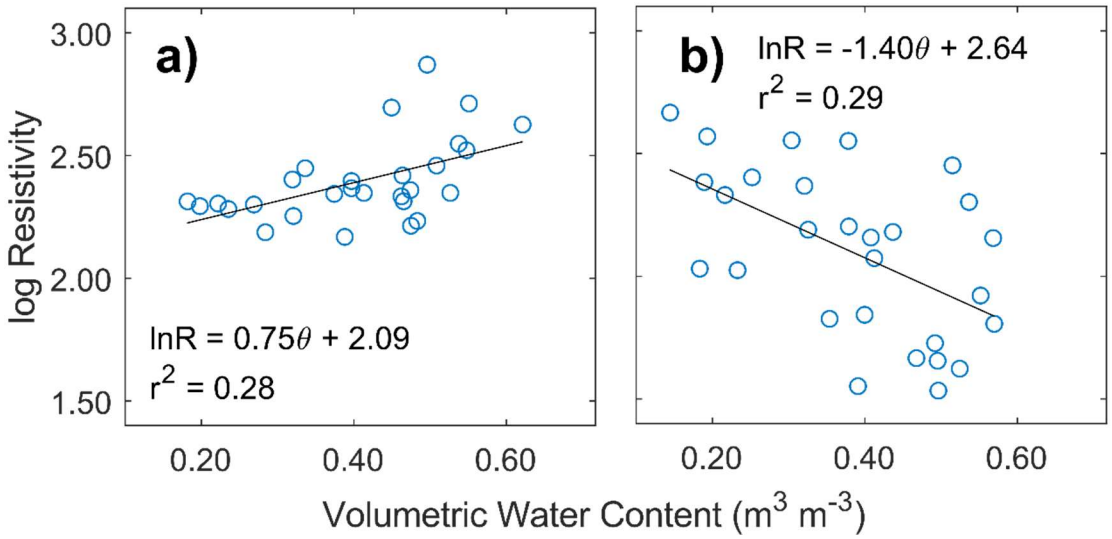


Figure 31: Data plots with regression lines for log resistivity vs. volumetric water content ($m^3$ $m^{-3}$), Brazos River Site transects a) 041613 and b) 042313.

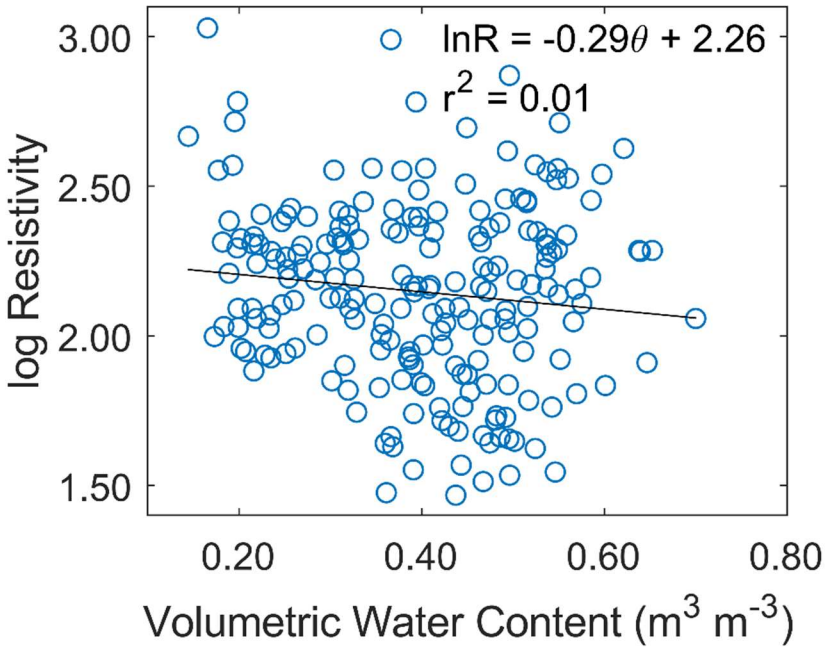


Figure 32: Data plot with regression line for log resistivity vs. volumetric water content ($m^3$ $m^{-3}$), all Brazos River Site transects.

Volumetric water and clay content were more highly correlated (Table 11). For combined BRS data, the $r^2$ value of 0.30 indicates that nearly one-third of the variability in volumetric water content can be explained by variation in clay content within the soil. The results of these regression models suggest that more can be surmised about water content from the clay content within the soil than from the log resistivity measured using ERT.

Table 11: Summary of volumetric water content vs. clay content linear regression models for individual and combined Brazos River Site transects.

| Transect | Slope | p-value | $r^2$ | DOF |
|---|---|---|---|---|
| **041113** | 6.33E-03 | 2.5E-06 | 0.39 | 45 |
| **041613** | 5.26E-03 | 0.11 | 0.20 | 12 |
| **041913** | 4.74E-03 | 1.3E-06 | 0.28 | 73 |
| **042313** | 5.70E-03 | 4.2E-03 | 0.18 | 42 |
| **042513E** | 4.72E-03 | 3.9E-06 | 0.31 | 58 |
| **042513W** | 6.04E-03 | 3.6E-16 | 0.42 | 121 |
| **Combined** | 5.27E-03 | <2E-16 | 0.30 | 361 |

Predicting volumetric water content by adding log resistivity to clay content data improves regression models, though the coefficient for log resistivity is not statistically significant for any of the MLR models (Table 12). Alpha values for clay content in transects 041113 and 041913 change from 0.001 to 0.01, while clay is still not shown to be statistically significant for 041613. The adjusted $r^2$ values for all transects show that

the MLR models improve on simple models, though only slightly for 041913. The value for 042313 increases from 0.16 (Table 11) to 0.63, and the $r^2$ for the BRS combined model increases from 0.30 to 0.50.

Table 12: Summary of volumetric water content vs. clay content and log resistivity multiple linear regression models for individual and combined Brazos River Site transects.

| Transect | Clay Slope | Clay p-value | lnR Slope | lnR p-value | $r^2$ | DOF |
|---|---|---|---|---|---|---|
| **041113** | 1.29E-02 | 9.95E-3 | 0.30 | 0.18 | 0.60 | 6 |
| **041613** | 1.11E-02 | 0.20 | 1.55 | 0.17 | 0.46 | 2 |
| **041913** | 4.71E-03 | 7.8E-3 | -0.09 | 0.37 | 0.28 | 17 |
| **042313** | 1.24E-02 | 4.9E-3 | 0.21 | 0.36 | 0.63 | 7 |
| **042513E** | 8.01E-03 | 7.0E-3 | -0.05 | 0.55 | 0.54 | 11 |
| **042513W** | 9.25E-03 | 2.7E-7 | -0.01 | 0.79 | 0.62 | 26 |
| **Combined** | 7.66E-03 | 5.3E-14 | -0.05 | 0.14 | 0.50 | 84 |

The degrees of freedom vary greatly between models for a given transect. Constructing the same models using only those data points for which log resistivity, volumetric water content, and clay content are available influences the results and reduces the variability in DOF from one model to the next (Table 13).

Trimming the data in the regression model for log resistivity vs. volumetric water content worsens the already poor relationships seen in Table 10. Since no clay data are available for transects 013113 and 040913, no models can be fit for these transects. For the remaining models (Table 13), $r^2$ values generally worsen, previously significant predictors become insignificant, and in one transect (040913), the sign of the slope

changes. The regression models for log resistivity and clay content are unaffected, as only a single data point is lost from among all of the transects.

Table 13: Summary of log resistivity vs. volumetric water content linear regression models for individual and combined Brazos River Site transects, for data points where log resistivity, volumetric water content, and clay content values are available.

| Transect | Slope | p-value | $r^2$ | DOF |
|---|---|---|---|---|
| **041113** | 0.05 | 0.91 | 0.00 | 7 |
| **041613** | 0.28 | 0.40 | 0.24 | 3 |
| **041913** | -0.23 | 0.65 | 0.01 | 18 |
| **042313** | -0.18 | 0.64 | 0.03 | 8 |
| **042513E** | -1.23 | 0.08 | 0.23 | 12 |
| **042513W** | -0.23 | 0.64 | 0.01 | 27 |
| **Combined** | -0.48 | 0.06 | 0.04 | 87 |

Of the regression models for predicting volumetric water content using clay content, all but one improve markedly by trimming the data set. The $r^2$ value for 041613 decreases from 0.20 in Table 11 to 0.13 in Table 14. The $r^2$ value for 042313, however, improves by nearly 0.50. The combined model value rises from 0.30 to 0.50.

Just as with MLR models fitted using full data sets, the trimmed data set models indicate that the relationship between clay content and water content is of primary importance. Adding log resistivity to the models summarized in Table 14 as an independent variable improves several of the models, as is demonstrated by adjusted $r^2$ values (Table 12) that are higher than corresponding simple model $r^2$ values. The results

of the trimmed MLR models are identical to the full MLR models summarized in Table 12, since the full set models already use data points with values for log resistivity, volumetric water content, and clay content.

Table 14: Summary of volumetric water content vs. clay content linear regression models for individual and combined Brazos River Site transects, for data points where log resistivity, volumetric water content, and clay content values are available.

| Transect | Slope | p-value | $r^2$ | DOF |
|---|---|---|---|---|
| **041113** | 1.11E-02 | 0.02 | 0.58 | 7 |
| **041613** | 4.93E-03 | 0.55 | 0.13 | 3 |
| **041913** | 4.53E-03 | 8.8E-03 | 0.32 | 18 |
| **042313** | 1.11E-02 | 3.8E-03 | 0.67 | 8 |
| **042513E** | 8.74E-03 | 1.1E-03 | 0.60 | 12 |
| **042513W** | 9.28E-03 | 1.5E-07 | 0.65 | 27 |
| **Combined** | 7.66E-03 | 2.5E-14 | 0.51 | 86 |

### *Dance Bayou*

Fewer data are available for the Dance Bayou site, where only two transects were measured compared to the eight measured at the BRS. The Dance Bayou measurements were also shallower, yielding fewer data points per core. Unlike BRS cores, all Dance Bayou cores were scanned using Vis/NIR to predict clay content. Accordingly, data points with values for log resistivity, volumetric water content, and clay content are used in all DB analysis.

Table 15: Summary of volumetric water content as a function of log resistivity linear regression models for individual and combined Dance Bayou transects.

| Transect | Slope | p-value | $r^2$ | DOF |
|---|---|---|---|---|
| **050813** | -0.44 | 0.26 | 0.05 | 26 |
| **050913** | -2.49 | 1.0E-05 | 0.49 | 29 |
| **Combined** | -2.47 | 1.0E-08 | 0.41 | 61 |
| **Combined trim** | -2.84 | 4.9E-10 | 0.47 | 60 |

Regression models for volumetric water content vs. log resistivity show that water content has a statistically significant impact on log resistivity for transect 050913 and the two transects combined at an alpha value of 0.001 (Table 15). An $r^2$ value of 0.51 for 050913 demonstrates that roughly half of the variation in water content can be explained by variation in log resistivity. The $r^2$ value for the combined model is lower at 0.41, but the slope is determined by the 050913 transect. For transect 050813, a single data point, denoted in Figure 33 by a red 'x,' heavily weights the regression model. While all other data points in this transect range in water content from approximately 0.40 $m^3\ m^{-3}$ to 0.60 $m^3\ m^{-3}$, this single point is 0.22 $m^3\ m^{-3}$. Data from transect 050913 have a slightly broader range in water content: roughly 0.30 to 0.60 $m^3\ m^{-3}$. The outlying data point coincides with the lowest clay content value for 050813 at 14.6%, which helps explain both its higher resistivity and lower water content values. Removing the sandy data point from the regression model increases the adjusted $r^2$ value from 0.41 to 0.47 and the p-value from 1.0E-08 to 4.9E-10 (Table 15).

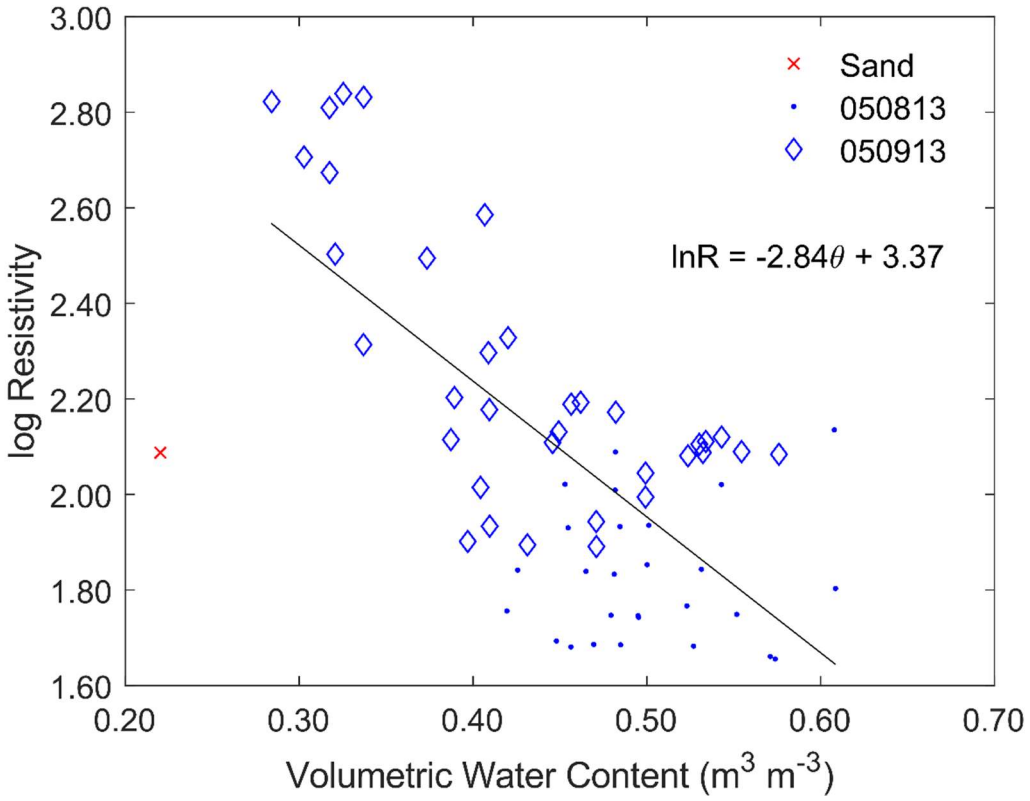


Figure 33: Data plot of log resistivity vs. volumetric water content ($m^3\ m^{-3}$), Dance Bayou transects 050813 and 050913 combined. Sandy data point from 050813 denoted by red 'x.' Regression model for combined data set with sandy point removed.

As with BRS data, the important relationship for DB data appears to be that between volumetric water content and clay content. The slopes for the 050813, 050913, and Combined models are all statistically significant at an alpha value of 0.001 (Table 16). The log resistivity vs. volumetric water content regression model for 050813 is a poor fit, but the 050813 model is the strongest for volumetric water content vs. clay content with an adjusted $r^2$ of 0.61. The adjusted $r^2$ value for 050913 is weaker for this

model at 0.44 than for log resistivity vs. volumetric water content at 0.49. The adjusted $r^2$ for the two data sets combined lies between those of the individual transects at 0.57.

Table 16: Summary of volumetric water content vs. clay content linear regression models for individual and combined Dance Bayou transects.

| Transect | Slope | p-value | $r^2$ | DOF |
|---|---|---|---|---|
| **050813** | 5.76E-03 | 6.3E-07 | 0.62 | 26 |
| **050913** | 4.74E-03 | 4.9E-05 | 0.44 | 29 |
| **Combined** | 5.23E-03 | 5.5E-12 | 0.57 | 57 |

Table 17: Summary of volumetric water content vs. clay content and log resistivity MLR models for individual and combined Dance Bayou transects.

| Transect | Clay Slope | Clay p-value | lnR Slope | lnR p-value | $r^2$ | DOF |
|---|---|---|---|---|---|---|
| **050813** | 5.67E-03 | 1.8E-06 | -0.03 | 0.68 | 0.59 | 25 |
| **050913** | 2.60E-03 | 3.1E-02 | -0.13 | 6.2E-03 | 0.54 | 28 |
| **Combined** | 4.22E-03 | 5.6E-07 | -6.29E-02 | 0.03 | 0.59 | 56 |

While the relationship between clay content and water content seems to be the most important among the regression models considered, DB log resistivity does have some importance. At the BRS, only clay content was shown to have a statistically significant relationship to water content (Table 14). For DB, however, log resistivity is also statistically significant in one transect and in combined data (Table 17). Incorporating log resistivity with clay content data in MLR raises the $r^2$ value from 0.41 for log resistivity vs. water content and 0.57 for water content vs. clay content to 0.59 for

the combined predictors. The alpha value at which the dependent variable is statistically significant in the combined data set MLR remains 0.001 for clay content, but changes from 0.001 to 0.05 for log resistivity.

These observations combined suggest that log resistivity data may be useful for estimating water content in a soil profile that is homogeneous in terms of the soil type – in this case, clay – but where variation in percent clay content within the layer is known.

*Combined Site Data*

Regression models were also evaluated by combining sites (Table 18). Volumetric water content is most simply modeled using clay content. A full model that uses both clay content and log resistivity data as predictors raises $r^2$ values slightly for all three data sets. Results of ANOVA that incorporates site (BRS vs. DB) into the full model as a dummy variable indicate that both site and clay content are significant predictors of water content at an alpha level of 0.001 while resistivity is not. These findings are consistent with the regression results in Table 18: expanding from the simple model, water content vs. clay content, to the full model, which includes log resistivity as an additional predictor, only marginally improves the $r^2$ values. Dividing the combined data set into site-specific data sets has a stronger effect on $r^2$ values. The dummy-variable ANOVA, used to test whether at least one of the slopes in the regression models is significantly different from the others, shows that the slopes for clay content are weakly significantly different (p-value < 0.05) while log resistivity slopes are not. Log resistivity has little to no additional predictive power for estimating volumetric water content of the soil.

Table 18: Comparison of statistcally significant (p-value <0.01) adjusted $r^2$ values for combined and individual site data.

| Model | Combined | Brazos River Site | Dance Bayou |
|---|---|---|---|
| $\boldsymbol{\theta \sim lnR}$ | 0.11 | | 0.36 |
| $\boldsymbol{\theta \sim}$ **Clay** | 0.46 | 0.49 | 0.56 |
| $\boldsymbol{\theta \sim}$ **Clay** $+$ **lnR** | 0.47 | 0.50 | 0.59 |

*Temporal Analysis*

Lastly, the data were analyzed over time to evaluate the effectiveness of ERT to monitor temporal changes in soil water content. The hypothesis is that changes in ERT data are in response to changes in water content since, over time in one space, clay content does not change. Models that use log resistivity to predict change in water content from similar locations across time yield mixed results (Table 19). Of the six groupings of data, only three have slopes significantly different from zero (p-value ≤ 0.05): Groups 3, 5, and 6. The slopes of all three models are negative; however, ANCOVA indicates that both the slopes (p-value = 0.03) and intercepts (p-value = 2.2E-04) of Groups 3 and 6 are different from each other. These three significant models have the largest changes in log resistivity and volumetric water content of the six data groupings analyzed. The $r^2$ value for Group 5, 0.10, may be lower than Groups 3 and 6 (0.69 and 0.39, respectively) because the intercept estimate for Group 5 was not significantly different from zero (p-value 0.86).

Temporal analysis also reveals that changes in ERT data do not reliably indicate the magnitude of changes in soil moisture. The largest decrease in resistivity, -96%,

corresponds to a change in water content of 0.31 to 0.40 $m^3 m^{-3}$. At the same time, one of the smallest changes in resistivity, 1%, corresponds to a 15% increase in water content of 0.32 to 0.38 $m^3 m^{-3}$. The largest increase in resistivity, 50%, corresponds to a decrease in water content of 0.40 to 0.35 $m^3 m^{-3}$. A 30% increase in resistivity results in a 0% change in water content for one data point. Resistivity data appear to be heavily influenced by noise that overwhelms the influence of water content on soil resistivity in wet Vertisols.

Since clay content data are available for some data points from Group 3, residuals from the Group 3 models were plotted against their corresponding changes in clay content. The $r^2$ value for this plot was 0.44 with a p-value of 0.22 and 3 degrees of freedom. Plotting residuals against clay content for BRS transect 041913 Core 20 was not significant, with an $r^2$ value of 0.02 and p-value of 0.61 on 12 degrees of freedom. This limited analysis suggests that neither clay content nor difference in clay content between data points is responsible for a quantifiable portion of the error.

The results suggest that it is possible that ERT could be used to estimate changes in water content over time. However, observing general trends is more appropriate than attempting to estimate quantitative changes. Additionally, small changes in resistivity should serve as a warning that change in water content values are likely poorly-estimated. It would be inappropriate to use ERT methods to evaluate change in water content during time periods of small changes in overall moisture content or when Vertisols are already high in water content.

Table 19: Summary of linear regression models for change in log resistivity vs. change in volumetric water content ($m^3 m^{-3}$) between different transects within groups.

| Group | Slope | Slope p-value | Intercept | Intercept p-value | $r^2$ | DOF | Max \|dR\| | Max \|dV\| |
|---|---|---|---|---|---|---|---|---|
| **1** | -0.02 | 0.70 | 3.31E-03 | 0.67 | -0.04 | 19 | 0.23 | 0.04 |
| **2** | -0.15 | 0.21 | 5.40E-02 | 0.26 | 0.16 | 5 | 0.62 | 0.06 |
| **3** | -0.25 | 2.1E-06 | -2.74E-02 | 7.5E-03 | 0.69 | 19 | 0.60 | 0.11 |
| **4** | 0.37 | 0.07 | 6.28E-02 | 5.5E-03 | 0.41 | 5 | 0.14 | 0.09 |
| **5** | -0.05 | 0.02 | 1.24E-03 | 0.86 | 0.10 | 40 | 0.68 | 0.13 |
| **6** | -0.07 | 5.4E-06 | 2.19E-02 | 1.7E-04 | 0.39 | 40 | 0.70 | 0.11 |

### *Potential Sources of Error*

Errors within the data and analyses described could have arisen from several sources. Clay content was predicted from Vis/NIR spectra. Waiser et al. (2007) noted bias in clay predictions from Vis/NIR spectra, and prediction models are known to underpredict clay content above 40%. Laboratory determinations of clay content may have been more accurate.

Temperature standardization and correction with depth could have introduced error for several reasons. Errors in historical weather data could have propagated error both in standardization and depth-correction. Measuring soil temperature throughout the depth of the profile measured, rather than relying on historical data, estimated parameters, and an empirical model to correct temperature based on depth, would likely have resulted in more accurate temperature, and therefore resistivity, data. The thermal diffusivity value used to correct with depth matches 80% of the data. Direct temperature

measurement would have obviated the need to estimate soil thermal diffusivity, removing this as a potential source of error.

# 4. CONCLUSIONS AND FUTURE WORK

The results of this study indicate that ERT data do not map to meaningful physical data in wet Vertisols. While general trends in soil profile and water content could be detected in transect images, the images themselves could not be interpreted accurately without knowledge of the site's physical properties. Transect images from the Brazos River Site generally show increasing resistivity in the lower halves of the transects, but this is likely caused by current passing through the alluvial sand underlaying the Ships clay more than variations in water content or clay content within the clay layer. The resolution limits of ERT measurements obscure the boundary between the two soil layers leading to increases in measured resistivity at the lower depths of the Ships clay.

Textural changes in the soil profile, such as silt pockets observed in the soil cores, at the Brazos River Site were not readily apparent in the transect images due to their small size. At the Dance Bayou, changes in soil texture and corresponding changes in volumetric water content on the eastern end of transect 050913 were large enough in physical space and in magnitude of change to register in the image.

In wet Vertisols, volumetric water content is better predicted by clay content than by log resistivity data. For both study sites, linear regressions between volumetric water content and clay content outperformed regressions between either of those variables and

log resistivity. Adding log resistivity as a predictor variable in a multiple linear regression improves only slightly over models with one predictor.

Analysis of Variance indicates that log resistivity data have virtually no impact on regression models once the dummy variable for site is included. This analysis further demonstrates that the regression models are site specific. Site and clay content are the two strongest predictors in regression analysis conducted across the two sites. For regression models without the dummy variable, log resistivity improves the adjusted $r^2$ values achieved by clay content vs. water content models by a maximum of 0.03. Once the dummy variable is added, the presence of log resistivity data in any of the models considered improves the adjusted $r^2$ by no more than 0.01.

The two study sites each demonstrate wide ranges in clay content, occasionally including changes in soil classification, within their clay layers. The strong relationship between clay content and water content means that, without knowledge of the soil profile, distinguishing whether changes in resistivity result from movement of moisture within the profile or from variations in the clay content is impossible. Because soil texture in general influences how much water the soil can hold as well as the rate and direction water moves through the soil profile, changes in resistivity cannot be used to properly predict changes in water content without knowledge of the soil profile being considered.

Amidu and Dunbar (2007) noted, Ackerson et al. (2014) confirmed, and this study agrees, that large changes in soil moisture result in small changes in resistivity in wet clay soils. The slight slope that maps resistivity to water content in wet Vertisols is

easily overcome by noise from any of several factors. Figure 24 demonstrates that the majority of data from this study fall within the range of water contents where Ackerson et al. (2014) found that changes of 0.10 $m^3$ $m^{-3}$ water content result in an 8% change in resistivity. Given the inverted resistivity have an RMSE of 5%, it is impossible to determine whether changes in resistivity are the result of changes in water content or of random error. The ERT method is not a reliable method for estimating water content in wet Vertisols, especially in the absence of knowledge about the soil profile being measured.

It may be possible to use ERT to estimate trends related to changing water content in Vertisols at different measurement times given appropriate constraints. A baseline knowledge of the soil profile is necessary, and subsurface features likely to have a strong influence on resistivity should be avoided. The soil must be low enough in moisture content that changes in moisture between measurement times will correspond to measurable changes in resistivity. Outside these bounds, it is unlikely that ERT methods can be used to estimate changes in soil moisture. Additional studies could explore the thresholds at which accurate measurements can be made for different soil types.

Given the poor ability to map changes in resistivity to changes in volumetric water content at different measurement times, ERT is not well-suited to monitoring soil moisture in Vertisols suspected of being jurisdictional wetlands, such as those underlaying the Bottomland Hardwoods. Clay contents are too high and soils often too wet to model variations in water content using ERT.

Incorporating impedances at multiple frequencies has been shown to yield conductivity (the reciprocal of resistivity) as well as dielectric properties of soil (Bobrov et al., 2015; Logsdon, 2005; Rao et al., 2007; Smith-Rose, 1933). Further research into employing and interpreting complex impedance methods in situ may prove more effective than relying on DC resistivity in wet Vertisols. The additional data provided by these techniques may enable extraction of soil texture, macrostructures, and water content. This may require new or modified measurement systems, as well as new inversion techniques, to be successful.

# REFERENCES


Ackerson, J.P., McInnes, K.J., Morgan, C.L.S., Everett, M.E., 2017. Measuring crack porosity using three-dimensional electrical resistivity tomography. Soil Sci. Soc. Am. J. 81, 1025–1035. doi:10.2136/sssaj2016.10.0353

Ackerson, J.P., Morgan, C.L.S., Everett, M.E., McInnes, K.J., 2014. The Role of Water Content in Electrical Resistivity Tomography of a Vertisol. Soil Sci. Soc. Am. J. 78, 1552–1562. doi:10.2136/sssaj2014.01.0032

Advanced Geosciences, 2009. Instruction Manual for EarthImager 2D Version 2.4.0 Resisitivity and IP Inversion Software.

Advanced Geosciences, 2008. Instruction Manual for EarthImager 3D Resistivity Inversion Software.

Advanced Geosciences, 2006. Instruction Manual for The SuperSting ™ with Swift ™ automatic resistivity and IP system.

Allen, P.M., Harmel, R.D., Arnold, J., Plant, B., Yelderman, J., King, K., 2005. Field data and flow system response in clay (vertisol) shale terrain, north central Texas, USA. Hydrol. Process. 19, 2719–2736. doi:10.1002/hyp.5782

Amidu, S.A., Dunbar, J.A., 2007. Geoelectric Studies of Seasonal Wetting and Drying of a Texas Vertisol. Vadose Zo. J. 6, 511–523. doi:10.2136/vzj2007.0005

Archie, G., 1942. The electrical resistivity log as an aid in determining some reservoir characteristics. Trans. AIME 146, 54–62. doi:10.2118/942054-G

Ashworth, J.B., Hopkins, J., 1995. Aquifers of Texas, Texas Water Development Board. Austin, Texas.

Bobrov, P.P., Repin, A.V., Rodionova, O.V., 2015. Wideband Frequency Domain Method of Soil Dielectric Property Measurements. Geosci. Remote Sensing, IEEE Trans. 53, 2366–2372. doi:10.1109/TGRS.2014.2359092

Campbell, G.S., Norman, J.M., 1998. Environmental Biophysics, 2nd ed. Springer Science+Business Media, Inc., New York, NY.

Cardenas, M.B., Kanarek, M.R., 2014. Soil moisture variation and dynamics across a wildfire burn boundary in a loblolly pine (Pinus taeda) forest. J. Hydrol. 519, 490–502. doi:10.1016/j.jhydrol.2014.07.016

Chanasyk, D.S., Naeth, M.A., 1996. Field measurement of soil moisture using neutron probes. Can. J. Soil Sci. 76, 317–323. doi:10.4141/cjss96-038

Constable, S., Parker, R., Constable, C., 1987. Occam's inversion: A practical algorithm for generating smooth models from electromagnetic sounding data. Geophysics 52, 289–300.

Dahlin, T., 2001. The development of DC resistivity imaging techniques. Comput. Geosci. 27, 1019–1029.

Dahlin, T., Zhou, B., 2004. A numerical comparison of 2D resistivity imaging with 10 electrode arrays. Geophys. Prospect. 52, 379–398. doi:10.1111/j.1365-2478.2004.00423.x

Dinka, T.M., Morgan, C.L.S., McInnes, K.J., Kishné, A.S., Daren Harmel, R., 2013. Shrink-swell behavior of soil across a Vertisol catena. J. Hydrol. 476, 352–359.

doi:10.1016/j.jhydrol.2012.11.002

Everett, M., 2013a. Electrical resistivity method, in: Near-Surface Applied Geophysics. Cambridge University Press, New York, NY, pp. 86–119.

Everett, M., 2013b. Linear Inversion, in: Near-Surface Applied Geophysics. Cambridge University Press, New York, NY, pp. 336–356.

Evett, S.R., Tolk, J. a., Howell, T. a., 2003. A Depth Control Stand for Improved Accuracy with the Neutron Probe. Vadose Zo. J. 2, 642. doi:10.2136/vzj2003.0642

Evett, S.R., Tolk, J.A., Howell, T.A., 2006. Soil Profile Water Content Determination. Vadose Zo. J. 5, 894. doi:10.2136/vzj2005.0149

Ge, Y., Morgan, C.L.S., Ackerson, J.P., 2014. VisNIR spectra of dried ground soils predict properties of soils scanned moist and intact. Geoderma 221–222, 61–69. doi:10.1016/j.geoderma.2014.01.011

George, P.G., Mace, R.E., Petrossian, R., 2011. Aquifers of Texas, Texas Water Development Board. Austin, Texas.

Green, D.A., 2011. A colour scheme for the display of astronomical intensity images. Bull. Astron. Soc. India 39, 289–295.

Hayley, K., Bentley, L.R., Gharibi, M., Nightingale, M., 2007. Low temperature dependence of electrical resistivity: Implications for near surface geophysical monitoring. Geophys. Res. Lett. 34, 1–5. doi:10.1029/2007GL031124

Jacob, J.S., Griffin, R.W., Miller, W.L., Wilding, L.P., 1997. Aquerts and Aquertic Soils : A Querulous Proposition, in: Vepraskas, M., Sprecher, W. (Eds.), Aquic Conditions and Hydric Soils: The Problem Soils. Soil Science Society of America,

Madison, Wisconsin, pp. 61–77.

Jayawickreme, D.H., Dam, R.L. Van, Hyndman, D.W., 2008. Subsurface imaging of vegetation , climate , and root-zone moisture interactions 35, 1–5. doi:10.1029/2008GL034690

Keller, G. V., Frischknecht, F.C., 1966. Electrical methods in geophysical prospecting. Pergamn Press, Oxford, UK.

Kilmer, V.J., Alexander, L.T., 1949. Methods of Making Mechanical Analyses of Soils. Soil Sci. 68, 15–24. doi:10.1097/00010694-194907000-00003

LaBrecque, D.J., Yang, X., 2001. Difference inversion of ERT data: A fast inversion method for 3-D in situ monitoring. J. Environ. Eng. Geophys. 6, 83–89.

Logsdon, S.D., 2005. Soil Dielectric Spectra from Vector Network Analyzer Data. Soil Sci. Soc. Am. J. 69, 983. doi:10.2136/sssaj2004.0352

Loke, M.H., Barker, R.D., 1996. Rapid least-squares inversion of apparent resistivity pseudosections by a quasi-Newton method. Geophys. Prospect. 44, 131–152. doi:10.1111/j.1365-2478.1996.tb00142.x

Mausbach, M.J., Parker, W.B., 2001. Background and History of the Concept of Hydric Soils, in: Richardson, J.L., Vepraskas, M.J. (Eds.), Wetland Soils: Genesis, Hydrology, Landscapes, and Classification. Lewis Publishers, pp. 19–33.

Michot, D., Benderitter, Y., Dorigny, A., Nicoullaud, B., King, D., Tabbagh, A., 2003. Spatial and temporal monitoring of soil water content with an irrigated corn crop cover using surface electrical resistivity tomography. Water Resour. Res. 39, n/a-n/a. doi:10.1029/2002WR001581

Miller, C.R., Routh, P.S., Brosten, T.R., McNamara, J.P., 2008. Application of time-lapse ERT imaging to watershed characterization. Geophysics 73, G7–G17.

Miller, W., Bragg, A., 2007. Soil characterization and hydrological monitoring project, Brazoria County, Texas, bottomland hardwood Vertisols, USDA, NRCS, Temple. Temple, Texas.

Munster, C., Mathewson, C., Wrobleski, C., 1996. The Texas A&M University Brazos River hydrogeologic field site. Environ. Eng. Geosci. 2, 517–530.

Neely, H.L., Ackerson, J.P., Morgan, C.L.S., McInnes, K.J., 2014. Instrumentation to Measure Soil Subsidence and Water Content in a Single Borehole. Soil Sci. Soc. Am. J. 78, 1251. doi:10.2136/sssaj2014.02.0055n

R Core Team, 2017. R: A Language and Environment for Statistical Computing.

Rao, B.H., Bhat, A.M., Singh, D.N., 2007. Application of impedance spectroscopy for modeling flow of AC in soils. Geomech. Geoengin. 2, 197–206. doi:10.1080/17486020701466778

Rappaport, C., 2002. A color map for effective black-and-white rendering of color-scale images. IEEE Antennas Propag. Mag. 44, 94–96. doi:10.1109/MAP.2002.1028735

Rein, A., Hoffmann, R., Dietrich, P., 2004. Influence of natural time-dependent variations of electrical conductivity on DC resistivity measurements. J. Hydrol. 285, 215–232. doi:10.1016/j.jhydrol.2003.08.015

Shah, S., Kress, W., Legchenko, A., 2007. Application of Surface Geophysical Methods, With Emphasis on Magnetic Resonance Soundings, to Characterize the Hydrostratigraphy of the Brazos River Alluvium Aquifer, College Station, Texas,

July 2006--a Pilot Study. Reston, Virginia.

Sheather, S.J., 2009. Multiple Linear Regression, in: A Modern Approach to Regression with R. Springer Science+Business Media, Inc., New York, NY, pp. 125–146.

Smith-Rose, R.L., 1933. Electrical Measurements on Soil with Alternating Currents. J. Inst. Electr. Eng. 75, 221–237. doi:10.1049/jiee-1.1934.0127

Soil Survey Staff, 1999. Soil Taxonomy: A Basic System of Soil Classification for Making and Interpreting Soil Surveys. Agric. Handb. doi:10.1017/S0016756800045489

The MathWorks Inc., 2018. MATLAB Release 2018a.

TWC Product and Technology LLC, 2018. Weather Underground [WWW Document]. URL https://www.wunderground.com/history/

U.S. Army Corps of Engineers, 2010. Regional Supplement to the Corps of Engineers Wetland Delineation Manual: Atlantic and Gulf Coastal Plain Region. Vicksburg, Mississippi.

U.S. Fish & Wildlife Service, 2018. San Bernard Refuge Map [WWW Document]. URL https://www.fws.gov/refuge/San_Bernard/map.html

U.S. Fish & Wildlife Service, 2013. Texas Mid-coast National Wildlife Refuge Complex - Comprehensive Conservation Plan and Environmental Assessment.

Waiser, T.H., Morgan, C.L.S., Brown, D.J., Hallmark, C.T., 2007. In Situ Characterization of Soil Clay Content with Visible Near-Infrared Diffuse Reflectance Spectroscopy. Soil Sci. Soc. Am. J. 71, 389–396. doi:10.2136/sssaj2006.0211

Wenner, F., 1915. A method of measuring earth resistivity. Bull. Bur. Stand. 12, 469–478.

Wrobleski, C., 1996. An Aquifer Characterization at the Texas A & M University Brazos River Hydrologic Field Site, Burleson Co., Texas. Texas A&M University.

Yeh, T.-C.J., Liu, S., Glass, R.J., Baker, K., Brainard, J.R., Alumbaugh, D., LaBrecque, D., 2002. A geostatistically based inverse model for electrical resistivity surveys and its applications to vadose zone hydrology. Water Resour. Res. 38, 14-1-14–13. doi:10.1029/2001WR001204

Zhou, W., Beck, B., Stephenson, J., 2000. Reliability of dipole-dipole electrical resistivity tomography for defining depth to bedrock in covered karst terranes. Environ. Geol. 39, 760–766.

# APPENDIX I

# INVERSION SETTINGS

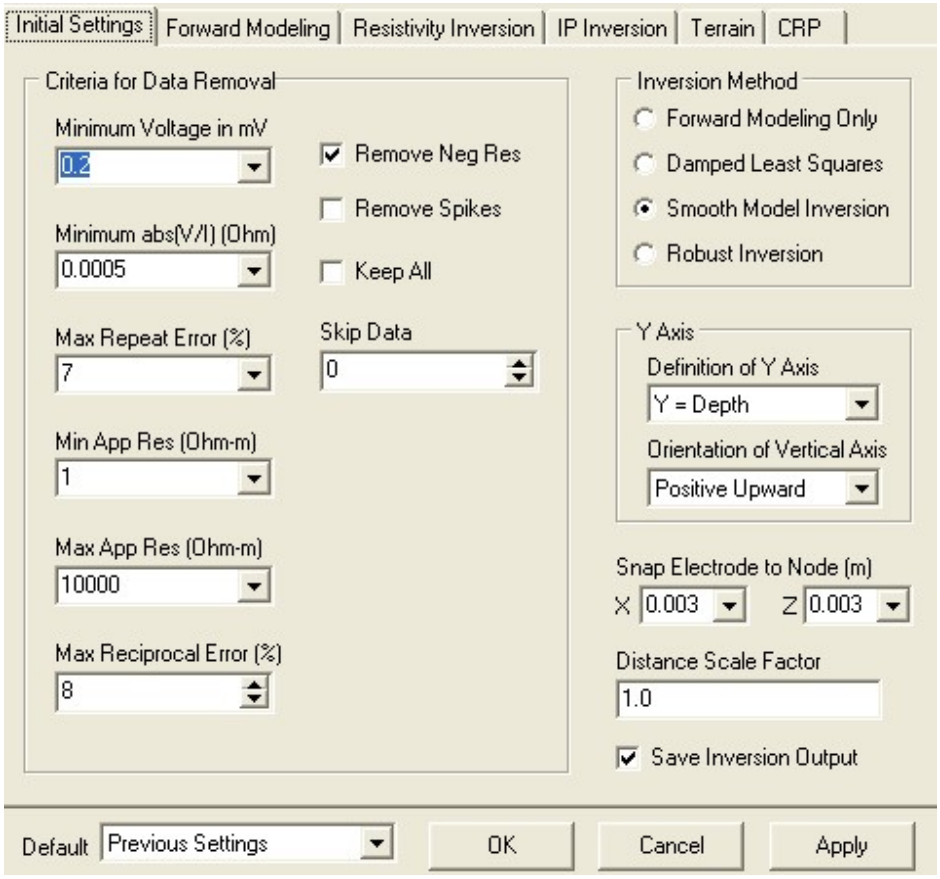


Figure 34: Initial Settings for EarthImager 2D inversions.

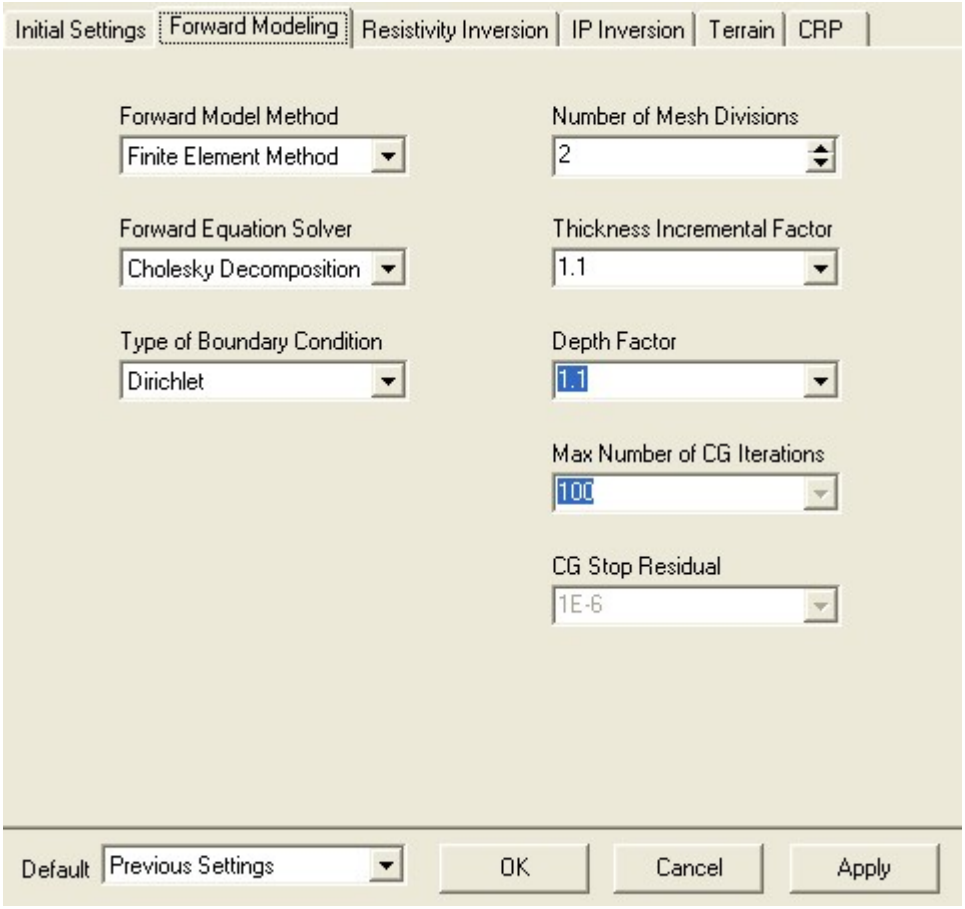


Figure 35: Forward Modeling Settings for EarthImager 2D inversions.

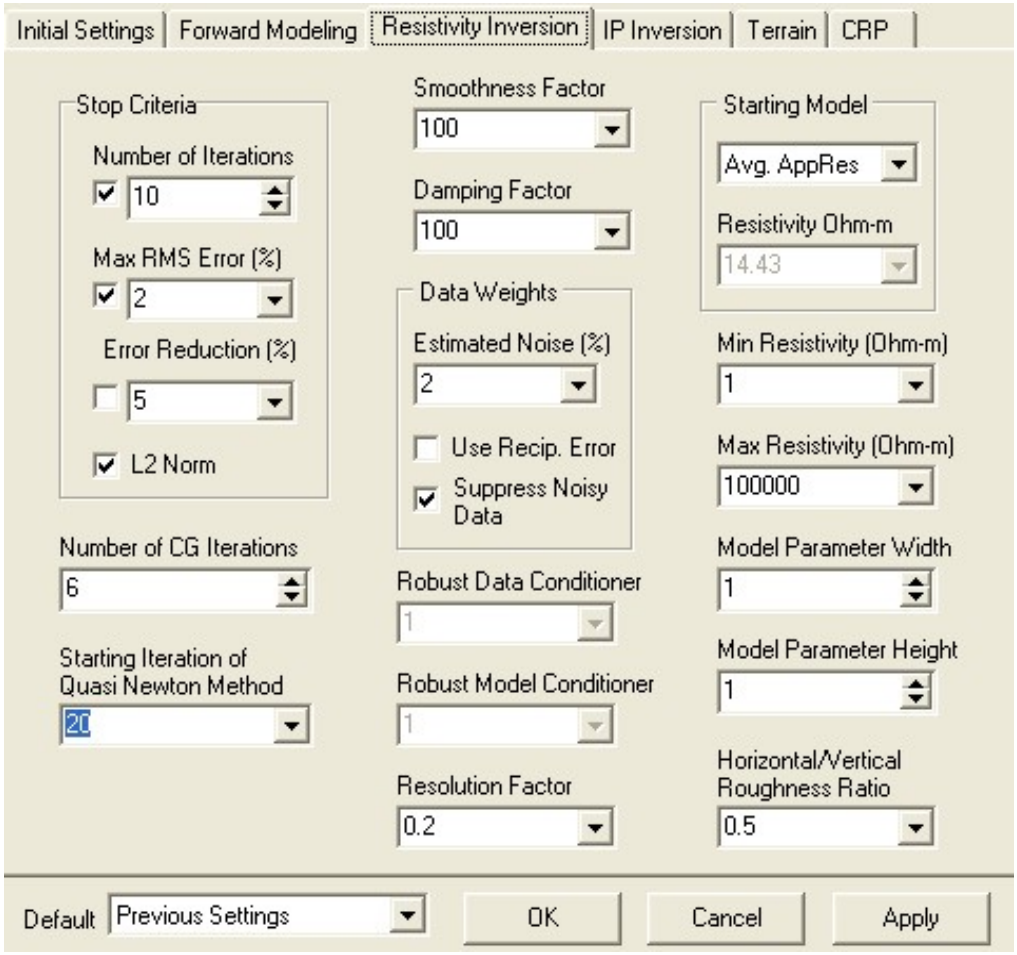


Figure 36: Resistivity Inversion Settings for EarthImager 2D inversions.

IP Inversion, Terrain, and CRP settings did not apply to these surveys and were not used.

# APPENDIX II

# CLAY CONTENT FIGURES

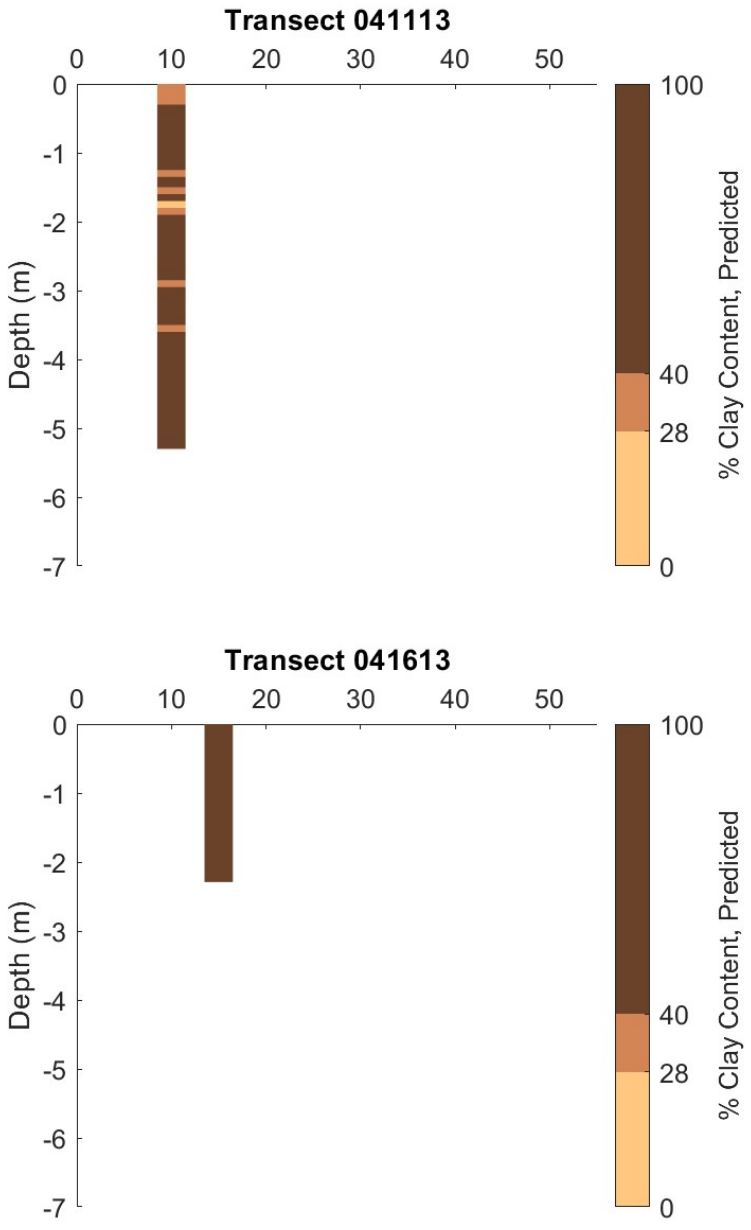
Transect 041113
0
10
20
30
40
50
0
-1
-2
-3
-4
-5
-6
-7
Depth (m)
100
40
28
0
% Clay Content, Predicted
Transect 041613
0
10
20
30
40
50
0
-1
-2
-3
-4
-5
-6
-7
Depth (m)
100
40
28
0
% Clay Content, Predicted

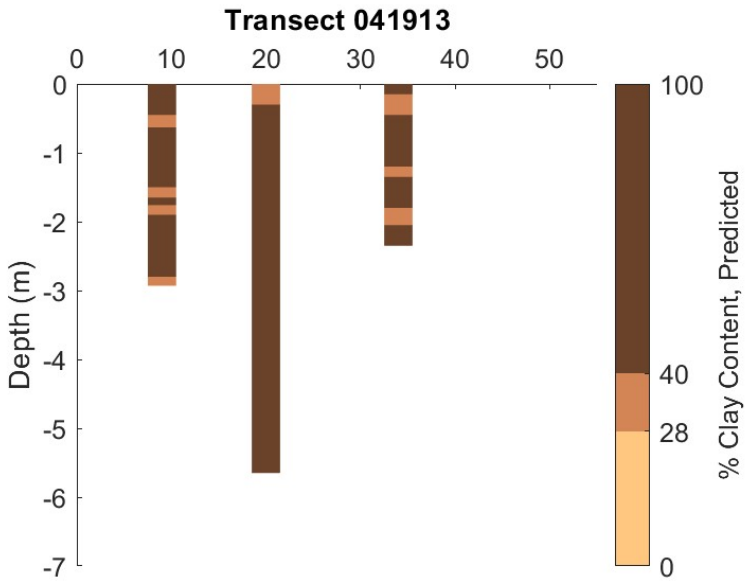
Transect 041913
0
10
20
30
40
50
0
-1
-2
-3
-4
-5
-6
-7
Depth (m)
100
40
28
0
% Clay Content, Predicted

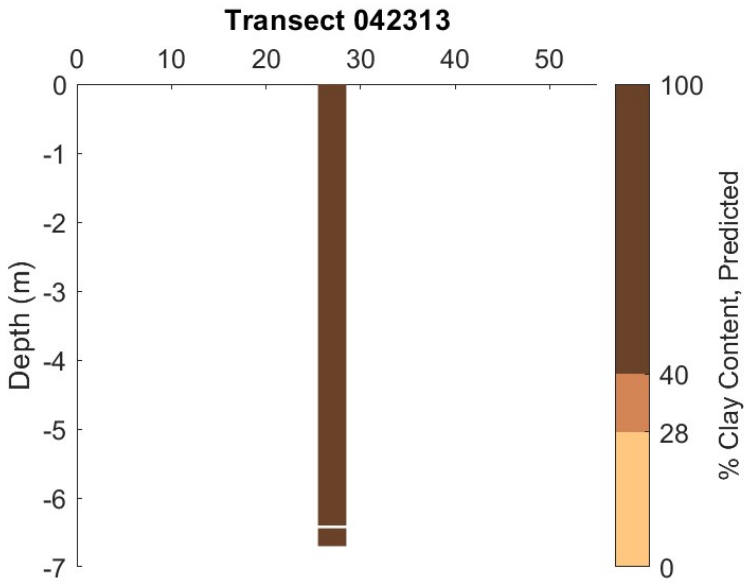
Transect 042313
0
10
20
30
40
50
0
-1
-2
-3
-4
-5
-6
-7
Depth (m)
100
40
28
0
% Clay Content, Predicted

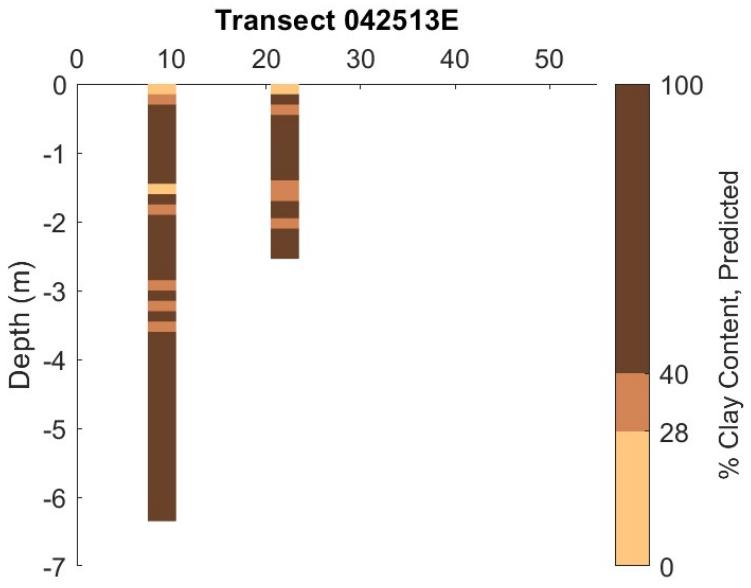
Transect 042513E
0
10
20
30
40
50
0
-1
-2
-3
-4
-5
-6
-7
Depth (m)
100
40
28
0
% Clay Content, Predicted

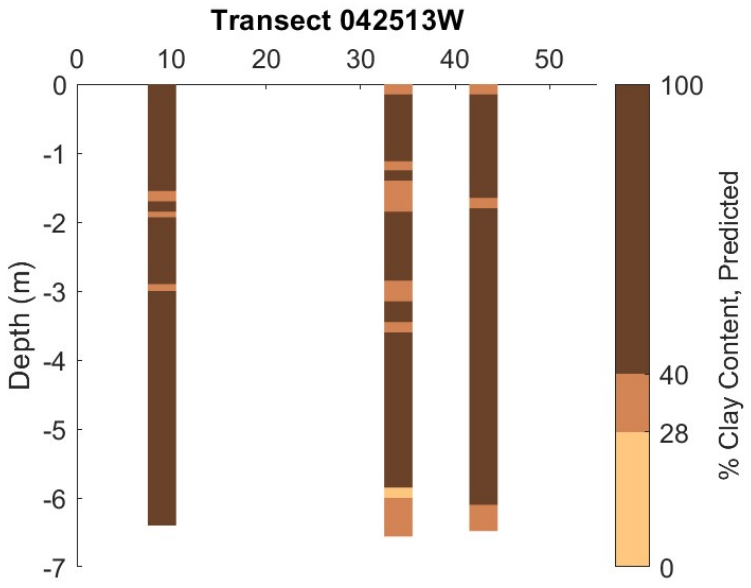
Transect 042513W
0
10
20
30
40
50
0
-1
-2
-3
-4
-5
-6
-7
Depth (m)
100
40
28
0
% Clay Content, Predicted

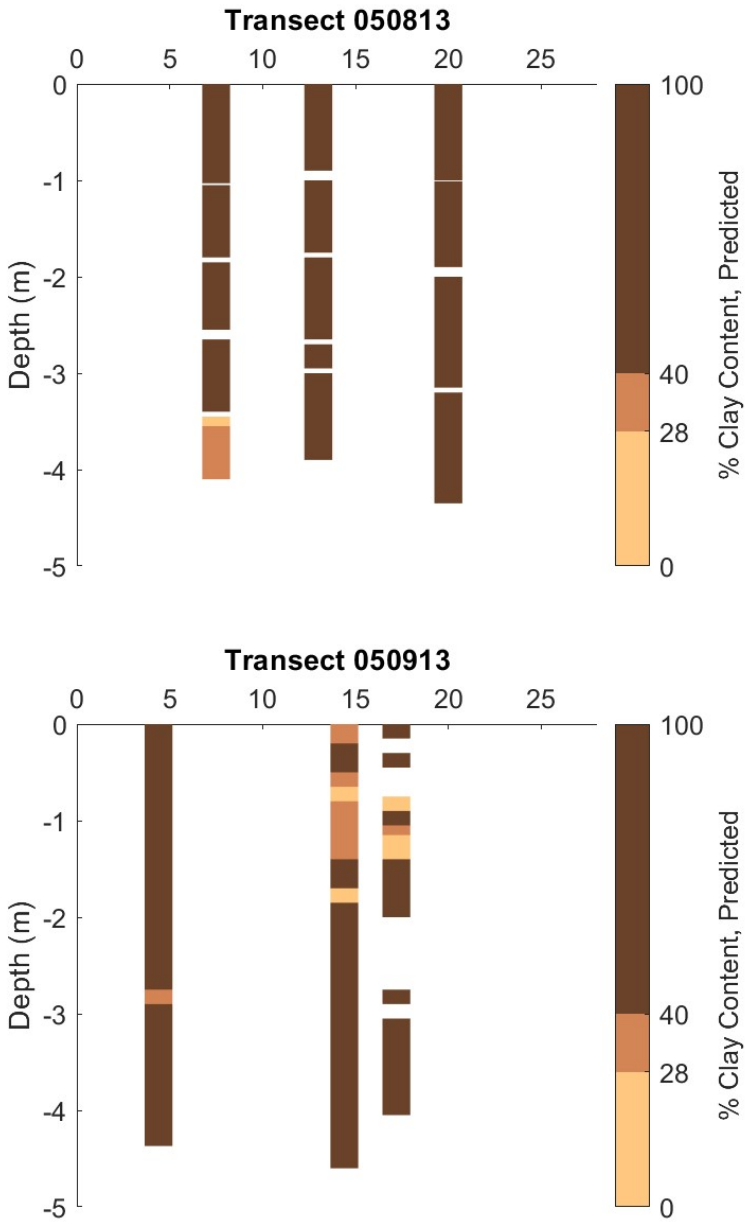
Transect 050813
0
5
10
15
20
25
0
-1
-2
-3
-4
-5
Depth (m)
100
40
28
0
% Clay Content, Predicted
Transect 050913
0
5
10
15
20
25
0
-1
-2
-3
-4
-5
Depth (m)
100
40
28
0
% Clay Content, Predicted